Oil & Natural Gas Technology

Detection and Production of Methane Hydrate

Semi-annual Progress Report

Reporting Period: July, 2008-October, 2008

Submitted by:
Rice University and University of Houston

George J. Hirasaki and Walter Chapman, Chemical and Biomolecular Engineering
Gerald R. Dickens, Colin A. Zelt, and Brandon E. Dugan, Earth Science
Kishore K. Mohanty, University of Houston

November, 2008

DOE Award No.: DE-FC26-06NT42960

Rice University – MS 362
6100 Main St.
Houston, TX 77251-1892
Phone: 713-348-5416; FAX: 713-348-5478; Email: gjh@rice.edu

University of Houston
Department of Chemical Engineering
4800 Calhoun Street
Houston, TX 77204-4004

Prepared for:
United States Department of Energy
National Energy Technology Laboratory

Office of Fossil Energy

Table of Contents

Disclaimer

Executive Summary

Task 5: Carbon Inputs and Outputs to Gas Hydrate Systems

Subtask 5.2 Constrain methane outputs using pore waters profiles and authigenic minerals. Additional recent articles have suggested that pore water sulfate profiles cannot be used to constrain upward methane fluxes in gas hydrate systems. This unanticipated notion challenges key assumptions in our modeling to date, and needs to be addressed. We have been recalculating constituent fluxes at numerous sites to ascertain this issue.

Task 6: Numerical Models for Quantification of Hydrate and Free Gas Accumulations

Subtask 6.1 Model Development. The simulator of geological scale accumulation of hydrate and free gas has been extended to 2-D and example simulations of heterogeneous systems are demonstrated. Heterogeneities result in regions of focus fluid flux. Higher hydrate and free gas are observed in the higher permeability regions as a result of the increased fluid flux.

Subtask 6.3 Compositional effects on BSR. BSR results from the sudden transition from hydrate to free gas. However, hydrate systems with multiple hydrocarbons can have a transition region where hydrate and free gas phases co-exist over tens of meters. This gradual transition results in attenuation of the amplitude of the reflection. The degree of attenuation is a function of the ratio of wave length of the signal to the length of the region of steep transition in acoustic impedance.

Task 7: Analysis of Production Strategy

Modeling of Warm Water Injection. The effect of depressurization and warm water injection was evaluated for a hydrate reservoir underlain by an infinite aquifer. Depressurization does not occur because of influx from the aquifer. Injection of warm water in beneficial due to dissociation of hydrate. There is diminishing improvement in recovery with increase in the temperature of the injected water.

Pore-Scale Model. A pore scale model which assumes that hydrate occupies the pore space by coating the pore walls predicts a higher permeability as a function of hydrate saturation compared to the Civan power-law model.

Task 8: Seafloor and Borehole Stability

We are moving forward on Task 8 as scheduled. We have begun integrating the sediment properties work (this task) with the geologic hydrate accumulation modeling (Task 6) by looking at how permeability and permeability anisotropy can be characterized over geologic time-scales and then incorporated in accumulation models. We are also assessing strength and pressure of sediment proposed for DOE-sponsored JIP hydrate work in the Gulf of Mexico; ultimately we are helping to develop a safe drilling program that will maximize our understanding of hydrate in the Gulf of Mexico and proved data for modeling these accumulations. We have also measured permeability to evaluate new

techniques for estimating permeability anisotropy and getting robust permeability data from logging measurements.

Task 9: Geophysical Imaging of Gas Hydrate and Free Gas Accumulations

For this task in particular, and others in general, we have successfully initiated collaboration with National Institute of Oceanography (NIO), India. We intend to demonstrate geophysical imaging with multichannel seismic data from the Krishna-Godavari (K-G) basin in the Indian east coast. NIO scientist, Dr. Pawan Dewangan, visited Rice University in the last week of July. During his visit Pawan presented examples highlighting the variations in the hydrate content. An interesting example is a case of three wells, 10, 12 and 13, drilled within 500 m range of each other that show rapidly varying hydrate concentration. While Well 10 encountered 128 m of hydrates, Well 12 and 13 encountered less than 60 m of massive hydrates. It was mutually agreed that modeling the seismic line closest to these three wells will be undertaken.

Priyank Jaiswal, now a post-doctoral research associate at Rice University, started working on the gas hydrate project officially, from September 15, 2008. Priyank traveled to NIO on September 29 and has been working on subtask 9.1 since then.

Background

A. Objective

This project seeks to understand regional differences in gas hydrate systems from the perspective of as an energy resource, geohazard, and long-term climate influence. Specifically, the effort will: (1) collect data and conceptual models that targets causes of gas hydrate variance, (2) construct numerical models that explain and predict regional-scale gas hydrate differences in 2- and 3-dimensions with minimal "free parameters", (3) simulate hydrocarbon production from various gas hydrate systems to establish promising resource characteristics, (4) perturb different gas hydrate systems to assess potential impacts of hot fluids on seafloor stability and well stability, and (5) develop geophysical approaches that enable remote quantification of gas hydrate heterogeneities so that they can be characterized with minimal costly drilling. Our integrated program takes advantage of the fact that we have a close working team comprised of experts in distinct disciplines.

The expected outcomes of this project are improved exploration and production technology for production of natural gas from methane hydrates and improved safety through understanding of seafloor and well bore stability in the presence of hydrates.

B. Scope of Work

The scope of this project is to more fully characterize, understand, and appreciate fundamental differences in the amount and distribution of gas hydrate and how this affects the production potential of a hydrate accumulation in the marine environment. The effort will combine existing information from locations in the ocean that are dominated by low permeability sediments with small amounts of high permeability sediments, one permafrost location where extensive hydrates exist in reservoir quality rocks and other locations deemed by mutual agreement of DOE and Rice to be appropriate. The initial ocean locations are Blake Ridge, Hydrate Ridge, Peru Margin and GOM. The permafrost location is Mallik. Although the ultimate goal of the project is to understand processes that control production potential of hydrates in marine settings, Mallik will be included because of the extensive data collected in a producible hydrate accumulation. To date, such a location has not been studied in the oceanic environment. The project will work closely with ongoing projects (e.g. GOM JIP and offshore India) that are actively investigating potentially economic hydrate accumulations in marine settings.

The overall approach is fivefold: (1) collect key data concerning hydrocarbon fluxes which is currently missing at all locations to be included in the study, (2) use this and existing data to build numerical models that can explain gas hydrate variance at all four locations, (3) simulate how natural gas could be produced from each location with different production strategies, (4) collect new sediment property data at these locations that are required for constraining fluxes, production simulations and assessing sediment stability, and (5) develop a method for remotely quantifying heterogeneities in gas hydrate and free gas distributions. While we generally restrict our efforts to the locations where key parameters can be measured or constrained, our ultimate aim is to make our efforts universally applicable to any hydrate accumulation.

Task 5: Carbon Inputs and Outputs to Gas Hydrate Systems

Subtask 5.1: Constrain organic carbon inputs using iodine

We have written a draft manuscript concerning iodine cycling in gas hydrate systems, and should have this revised and submitted by the end of the year. No additional progress on this subtask since the last report.

Subtask 5.2 Constrain methane outputs using authigenic minerals (and pore water profiles and carbon isotopes)

Anaerobic oxidation of methane (AOM) in shallow sediment represents a major loss of methane from all gas hydrate systems. In fact, it may be the dominant methane output from most systems, especially those with low rates of upward fluid advection.

In general, AOM occurs across a sulfate-methane transition (SMT), where upward moving methane reacts with downward diffusing sulfate. According to many authors, this reaction has a 1:1 stoichiometry ($CH_4 + SO_4^{2-} \rightarrow H_2O + HCO_3^- + HS^-$) and dominates dissolved sulfate and bicarbonate profiles in pore water (e.g., Borowski et al., 1999; Snyder et al., 2007). This concept is important to our work for two related reasons. First, because *in situ* methane concentrations and fluxes can be difficult to measure, upward methane fluxes could be determined from dissolved sulfate (or bicarbonate) fluxes into the SMT. Second, the depth of the SMT could be used to constrain the loss of methane and the abundance of underlying gas hydrate (Bhatnagar et al., 2008).

A series of recent articles, including one by Kastner and colleagues in the summer issue of “Fire in the Ice”, have argued against the above idea. Specifically, they suggest that dissolved sulfate and bicarbonate profiles cannot be used to constrain upward methane fluxes because compounds other than methane consume much of the sulfate in shallow sediment, even above gas hydrate systems. This idea, if correct, clearly impacts our work and modeling efforts. We have thus spent considerable time reevaluating data (including that generated as part of this project) in an effort to understand how and why various interpretations and assumptions concerning AOM and the SMT are incorrect.

We believe the problem lies in the use of concentrations instead of fluxes and the omission of bicarbonate from depth. Methanogenesis utilizes organic compounds to produce methane and bicarbonate. Consequently, there is an upward flux of both species, and the amount of bicarbonate added to the SMT is the sum of that produced by AOM and that rising from below. When the excess bicarbonate is accounted for, and the concentration profiles are converted to fluxes, the expected 1:1 flux relationship between sulfate and bicarbonate is observed (**Figure 5.1**).

We are presently writing a short article on this issue for the January “Fire in the Ice” and anticipate submitting a longer article in the coming months. We will then return to writing up our results from the Peru Margin. We have also just

obtained a suite of pore water samples collected from the Cascadia Margin by John Pohlman. We will analyze these over the next month for metals.

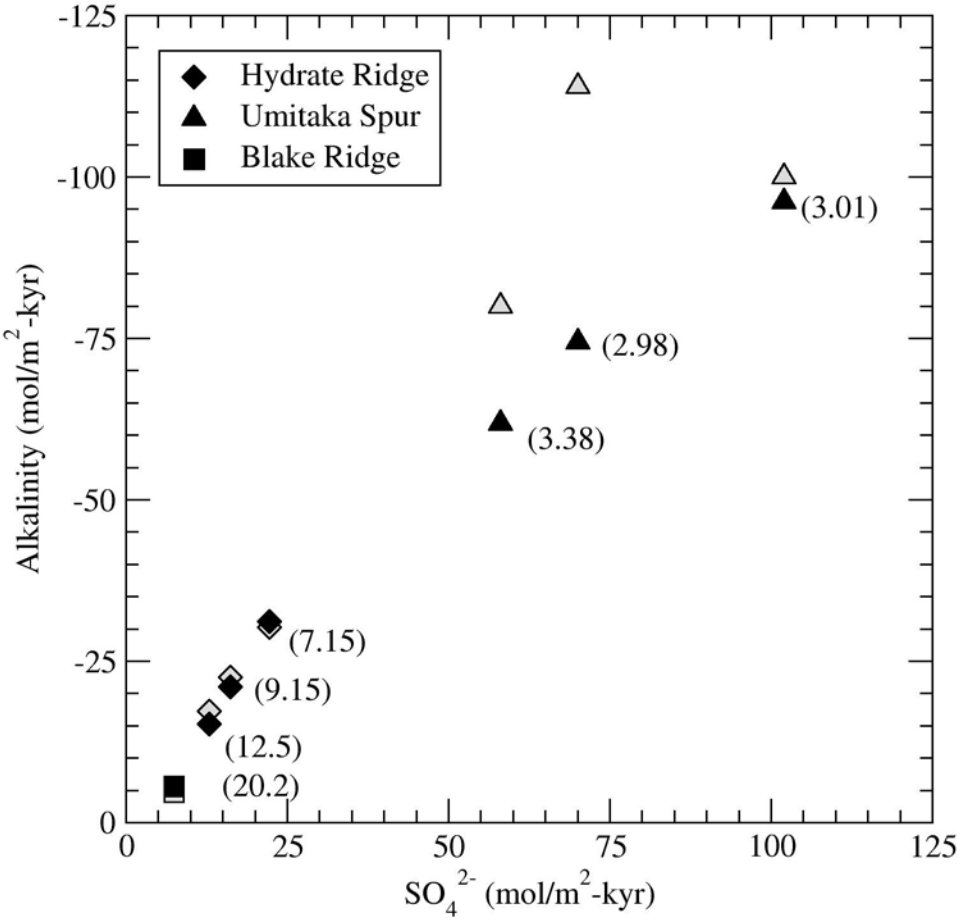

Figure 5.1: Calculated fluxes of sulfate and bicarbonate (alkalinity) across the SMT after correcting for upward flowing bicarbonate and carbonate precipitation at 6 sites (black), including the three discussed by Kastner and colleagues in their FITI article. Note the 1:1 relationship as expected for the case when AOM drives the sulfate and bicarbonate. Numbers refer to the depth of the SMT.

References

Borowski, W.S., C.K. Paull & W. Ussler III, 1999. Global and local variations of interstitial sulfate gradients in deep-water, continental margin sediments:

Sensitivity to underlying methane and gas hydrates. Marine Geology, 159: 131-154.
Snyder, G.T., A. Hiruta, R. Matsumoto, G.R. Dickens, H. Tomaru, R. Takeuchi, J. Komatsubara, Y. Ishida & H. Yu, 2007. Pore water profiles and authigenic mineralization in shallow marine sediments above the methane-charged system on Umitaka Spur, Japan Sea. Deep-Sea Research (II), 54: 1216-1239.

Hydrate Presentations

October 2008. Carbon cycling across the sulfate methane transition. Department of Earth Science, Rice University (faculty presentation)

October 2008. A global carbon cycle with seafloor methane. Department of Geosciences, Virginia Tech (Department seminar series)

Hydrate Activities

August 2008 – Dickens participated in the DOE gas hydrate evaluation held at NETL in Pittsburgh.

Task 6: Numerical Models for Quantification of Hydrate and Free Gas Accumulations

Subtask 6.1: Model Development

Accumulation of gas hydrate and free gas is modeled in heterogeneous marine sediments over geologic time scales. Our two-dimensional models incorporate deposition and compaction of heterogeneous sediment, methane generation, and migration of water with dissolved gas, so we can study how focused fluid flow through vertical fracture network systems and/or high permeability sand layers affect regional and local hydrate accumulation and saturation.

Fracture network systems, dipping sediment beds are common heterogeneities and fluid flow within natural gas hydrate systems are predominated primarily in these local fracture systems and high permeability sand layers, resulting in concentrated hydrate deposits. To incorporate these additional features and simulate realistic geologic systems, we extended our existing 1-D model (Bhatnagar et al, 2007) to 2-D model.

Gas hydrate systems with fractures

We simulate vertical fracture systems in our model, where we assign permeability in different grid blocks in a single column throughout our simulation domain as shown in figure 6.1.1 below.

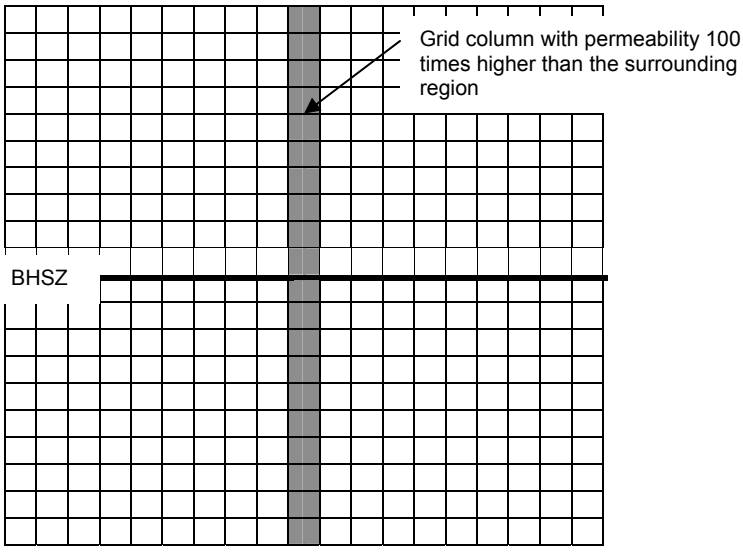

Figure 6.1-1: Permeability map showing initial location of a high permeability vertical fracture network system

We introduce a fracture system and follow the transient gas hydrate and free gas accumulation with sedimentation. Simulations with a vertical fracture network, 100 times more permeable than the surrounding formation that extends through the gas hydrate stability zone (GHSZ) up to the seafloor show focused fluid flow causing relatively higher hydrate and free gas saturation within the fracture network compared to the surrounding, lower permeability formation. The primary dimensionless transport parameters are defined as follows.

$$Pe_1 = \frac{U_{f,sed} L_c}{D_m} \qquad Da = \frac{\lambda L_c^2}{D_m} \qquad N_{gr} = \frac{k_0 \rho_w g}{\mu_w S} \qquad N_{hyp} = \frac{L_g}{L_c}$$

$$\beta = \frac{\alpha_0}{c^i_{m,eqb}} \qquad \gamma = \frac{1 - \phi_\infty}{\phi_\infty} \qquad \eta = \frac{\phi_0 - \phi_\infty}{1 - \phi_\infty} \qquad \hat{\phi} = \frac{\phi - \phi_\infty}{1 - \phi_\infty}$$

We observe that organic content leaving the GHSZ is dependent on the ratio Pe_1/Da as shown in figure 6.1.2.

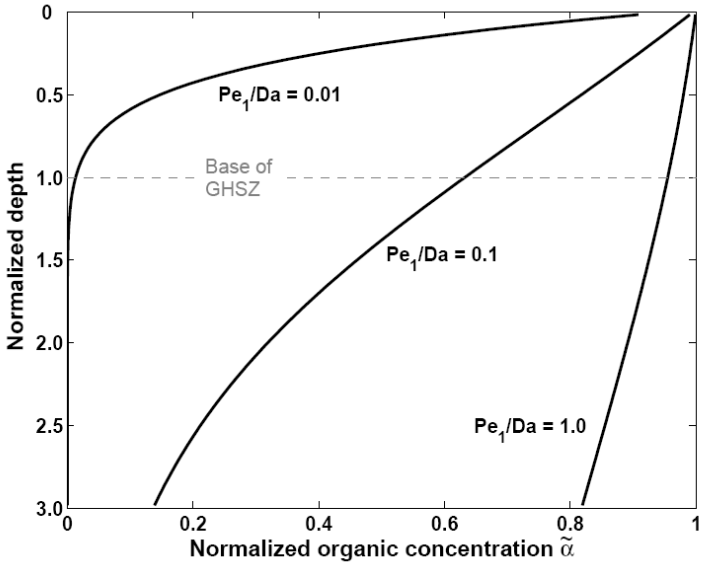

Figure 6.1.2: Normalized organic concentration profiles at steady state as a function of the ratio Pe_1/Da (Bhatnagar, 2007)

For lower values of Pe_1/Da (order of 10^{-2}), there is no organic material left for methane generation below the GHSZ. Larger values of Pe_1/Da results in considerable amount of organic material leaving the base of GHSZ. This allows the methane charged water to move upwards within the high permeability conduit to generate higher saturations of methane. In the following cases, we use $Pe_1/Da=0.1$, so as to have more organic content leaving the GHSZ for higher methane generation below the GHSZ.

In our model, Pe_1=0.1, Da=1, β=6, γ=9, η=6/9, $N_{t\varphi}$=1. Seafloor parameters, relative permeabilities, capillary pressure and physical properties of water, hydrate and free gas are the same as we used in our 1-D model (Bhatnagar 2007). The physical domain for all the simulation is normalized depth z ϵ [0, 2] and normalized lateral distance x ϵ [0, 2]. Dimensionless distance is defined with characteristic depth to the base of the GHSZ, L_t

$$\tilde{z} = \frac{z}{L_t} \quad , \quad \tilde{x} = \frac{x}{L_t}$$

Dimensionless time is defined by a combination of L_t and the methane diffusivity D_m

$$\tilde{t} = \frac{t}{L_t^2 / D_m}$$

We report the results at different dimensionless time as in figure 6.1.3 to 6.1.6. We have shown our results with varying ratio of vertical permeability to horizontal permeability (k_v/k_h) in the surrounding clay sediments. Anisotropic cases with lower ratio of k_v/k_h (order of 10^{-2}), show relatively higher hydrate saturations within the fracture network system because anisotropy focuses more of the fluid into the high permeability conduit. The flow is more prominent with lower realistic values of k_v/k_h. Table 6.1.1 is included which illustrates all the cases along with the parameters discussed in the report.

Table 6.1.1: Illustrates various cases along with the simulation parameters that were varied to explain the results below.

Figure	Cases	N_{sc}	k_v/k_h	Da	Pe_1/Da	Time	$N_{t\varphi}$
6.1.3	Continuous fracture system	20	1	1	0.1	0.6	1
6.1.4	Continuous fracture system	20	1	1	0.1	1.5	1
6.1.5	Continuous fracture system	20	10^{-2}	1	0.1	0.6	1
6.1.6	Continuous fracture system	20	10^{-2}	1	0.1	1.5	1

The location of the fracture system is represented by a set of dashed lines. We clearly observe a high focused flow along the high permeability conduit along the fracture system. The focused fluid flow is visualized by vector field plots and helps us to understand higher saturations of hydrate in these fracture systems. The color bars represent gas hydrate and free gas saturations. The broad white line at normalized depth z=1 represents the BHSZ.

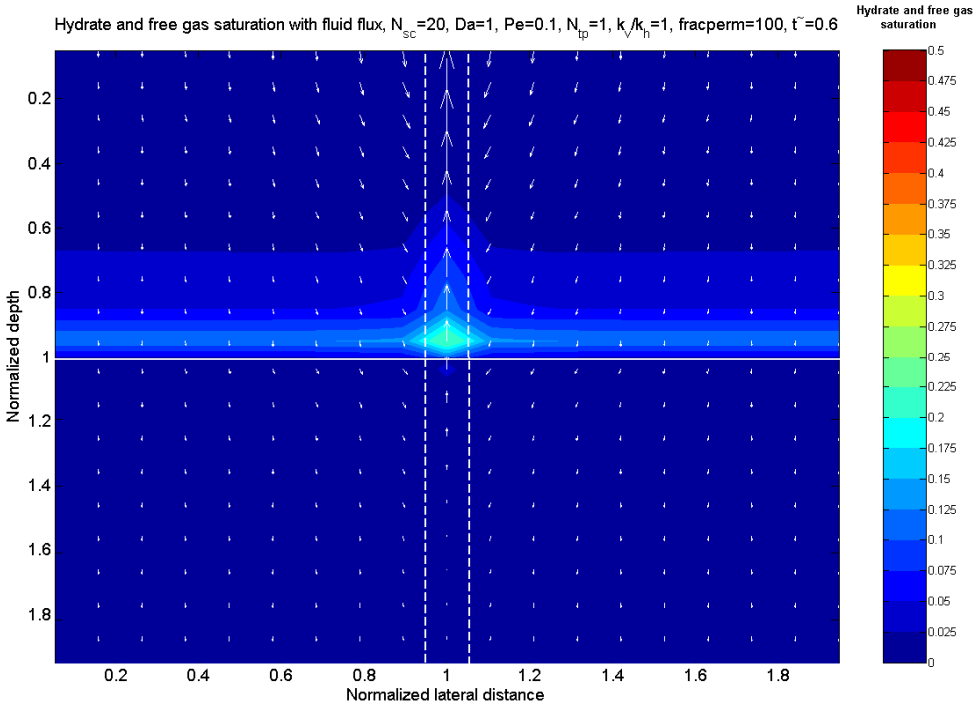

Figure 6.1.3: Gas hydrate and free gas saturation contours at dimensionless time t=0.6 for a continuous fracture system. Parameters: N_{sc} =20, k_v/k_h =1, Da=1, Pe_1/Da=0.1, $N_{t\varphi}$=1

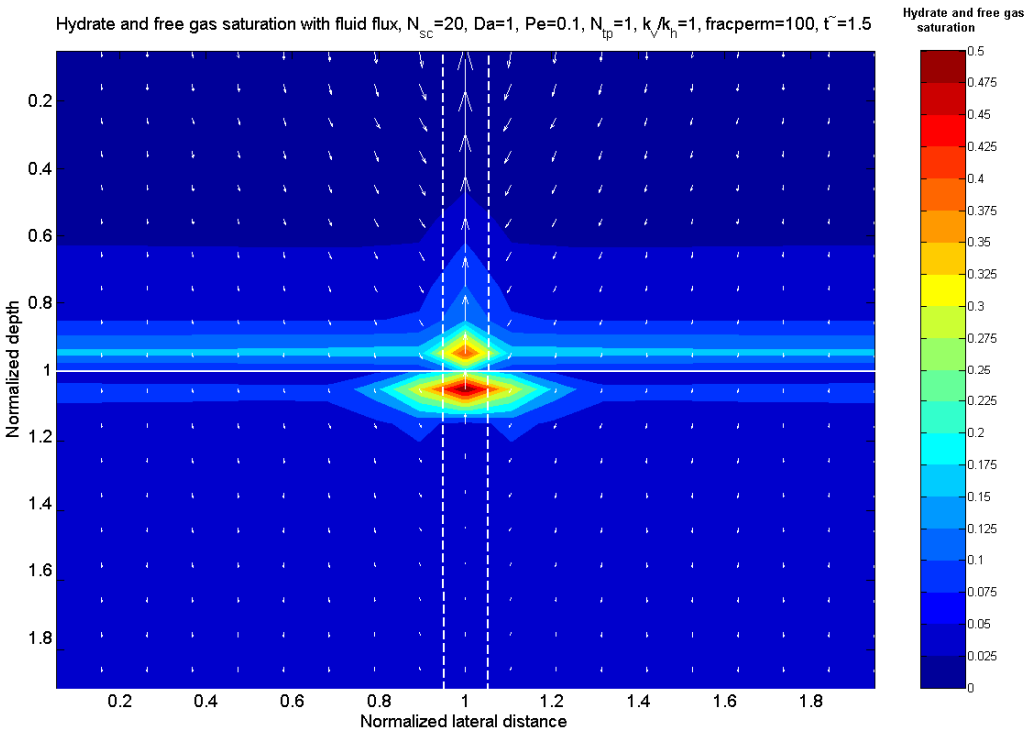

Figure 6.1.4: Gas hydrate and free gas saturation contours at dimensionless time t=1.5 for a continuous fracture system. Parameters: N_{sc} =20, k_v/k_h =1, Da=1, Pe_1/Da=0.1, $N_{t\varphi}$=1

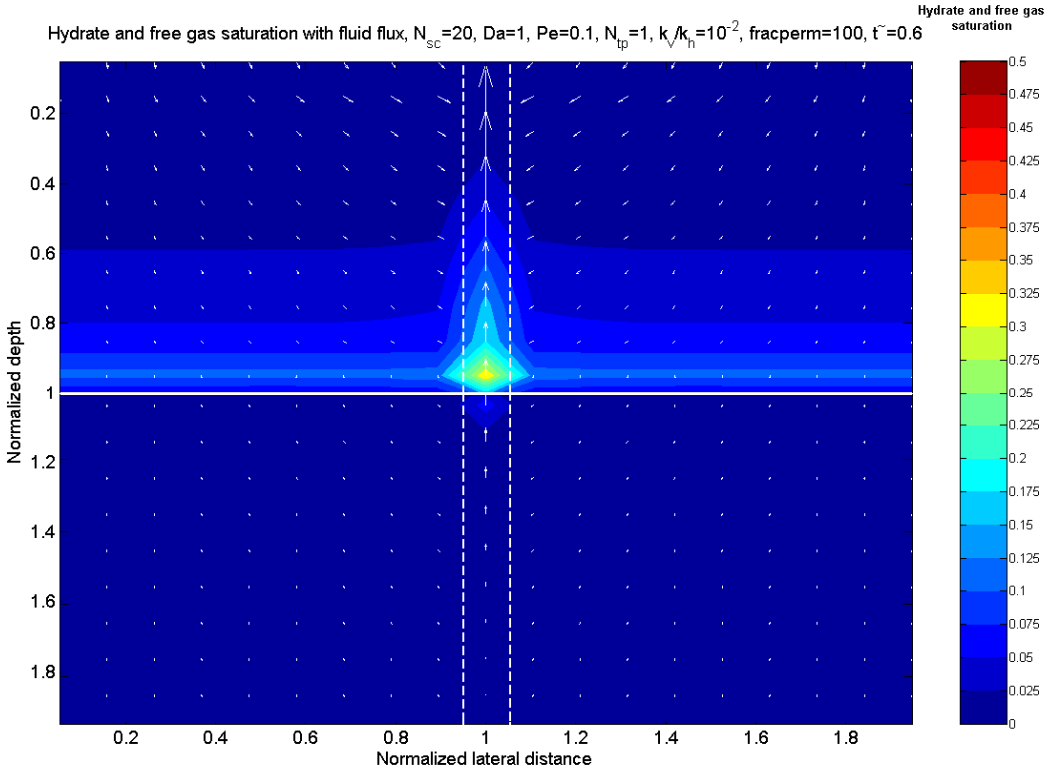

Figure 6.1.5: Gas hydrate and free gas saturation contours at dimensionless time t=0.6 for a continuous fracture system. Parameters: N_{sc}=20, k_v/k_h =10^{-2}, Da=1, Pe_1/Da=0.1, $N_{t\varphi}$=1

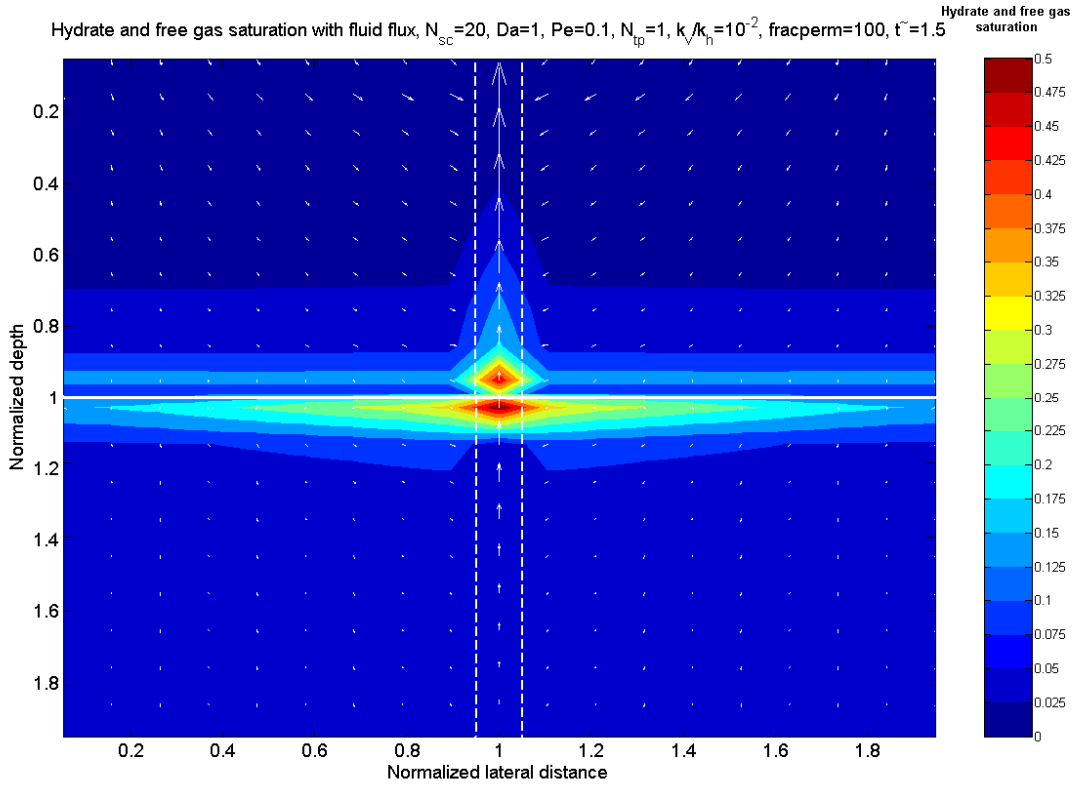

Figure 6.1.6: Gas hydrate and free gas saturation contours at dimensionless time t=1.5 for a continuous fracture system. Parameters: N_{sc} =20, k_v/k_h =10^{-2}, Da=1, Pe_1/Da=0.1, $N_{t\varphi}$=1

With passage of time, as the fracture moves out of the gas hydrate stability zone (GHSZ), hydrate distribution becomes more uniform along the lateral direction. Thus, we study the presence of vertical fracture systems with higher permeability, which significantly affects gas, hydrate and free gas distribution by focusing fluid flow along these fractures. Higher hydrate and free gas saturations are observed in the higher permeability fracture systems as a result of the increased fluid flux.

Gas hydrate systems with dipping sand layers

Our model also comprises of features to simulate high permeability dipping sand layers. Systems with dipping sand layers show similar localized, enhanced concentrations of hydrate and free gas within the high permeability conduits. In our case, we simulate a case with high permeability sand layers extending up to end of our simulation domain. We start with assigning high permeability to different grid blocks at a particular dip angle as shown below in figure 6.1.7. Similar to the fracture system case, the sand layer is assigned 100 times higher permeability than the surrounding clay matrix. The dimensionless parameter N_{sc}, which is the ratio of absolute permeability to the sedimentation rate, is 10 in the following cases. The downward movement of this sand layer and transient hydrate and gas saturations are recorded in time. The physical domain for all the simulation is z ϵ [0, 2] and x ϵ [0, 10]. The dimensionless parameters Pe_1=0.1, Da=10, β=6, γ=9, η=6/9, $N_{t\varphi}$=1. Sand layer deposits until dimensionless time t=0.5 and moves down at the same time. Hydrate and free gas saturation contours are shown in figure 6.1.8. The plot shows significant hydrate concentration within the sand layer. The focused fluid flow in high permeability sand layer is evident from the results shown. Free gas is also focused within the sand layer. We also observe uniform hydrate saturation along the lateral direction when the sand layer exits the system. We also show the fluid flux vector plots along with our saturation contour maps which help us to understand higher saturations in the high permeability sand layers. A set of dashed lines shows position of the sand layer within the low permeability clay matrix.

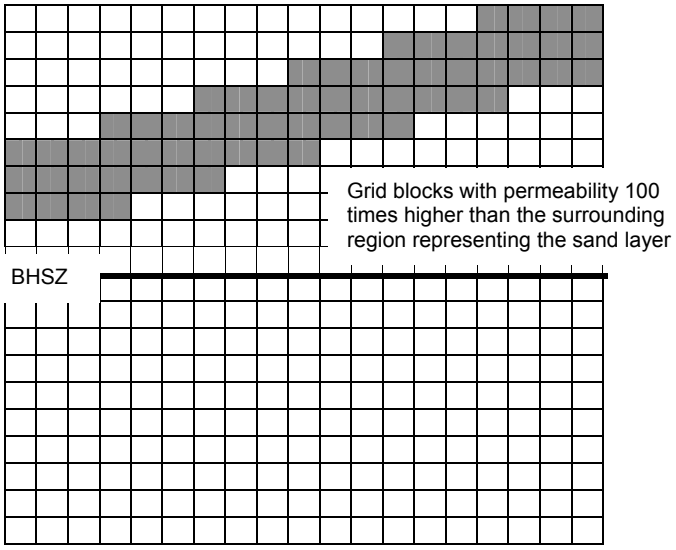

Figure 6.1.7: The initial permeability map schematic representing initial high permeability sand layers 100 times greater than the surrounding clay sediments.

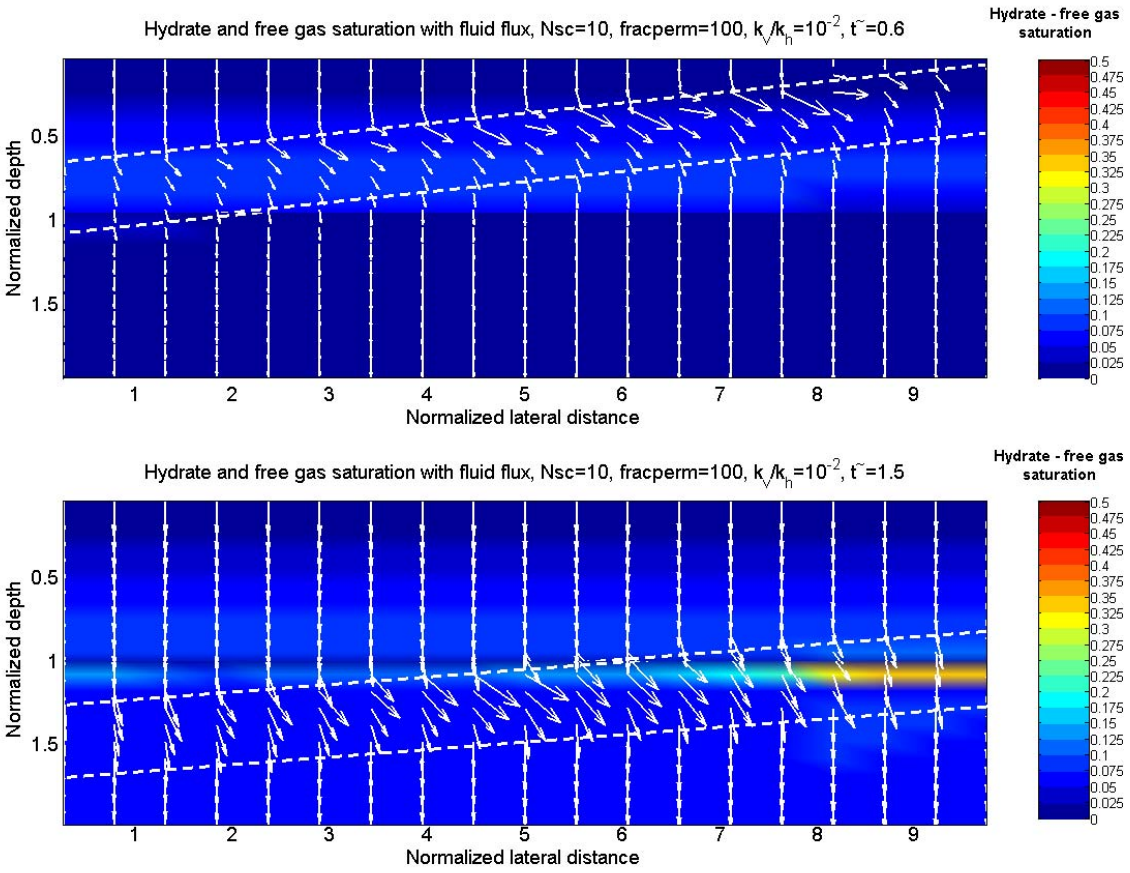

Figure 6.1.8: Gas hydrate and free gas saturation contours at dimensionless time t=0.6 and 1.5 for dipping sand layers. Parameters: N_{sc}=10, $k_v/k_h=10^{-2}$, Da=10, Pe_1/Da=0.01

Conclusions

A dimensionless 2-D model has been developed to simulate gas hydrate and free gas accumulation in marine sediments over geologic timescales. We studied the fluid flux with the help of quiver plots. In our previous **one-dimensional** work, we found that the accumulated hydrate saturation was dependent on Peclet number, Pe, which is the ratio of convective flux to the diffusive flux of methane. In our current two-dimensional work, it is the **local** convective flux relative to diffusion that determines the magnitude of hydrate and free gas saturation.

Future Work

We have incorporated heterogeneity in the form of fracture network systems and high permeability sand layers in our model. All this was achieved by just considering biogenic sources in the model. We can expect more gas hydrate saturations by incorporating external upward flux U_{ext} in our model as in our 1-D model. We also wish to model realistic geologic systems with our code. Effect of different parameters, combination of fracture systems cut through high permeability sand beds, has been planned for future work. We also aim to study

the hydrate accumulation with the help of sulfate methane transition as a tool. We also wish to study the distribution of hydrates in Krishna-Godavari basin and Mahanadi basin in collaboration with a group from NIO, India.

References

Bhatnagar G., PhD. Thesis (2008), *Accumulation of gas hydrates in marine sediments*, 10, p 192-236

Bhatnagar, G., Chapman, W.G., Dickens, G.R., Dugan, B. and Hirasaki, G.J.(2007). *Generalization of gas hydrate distribution and saturation in marine sediments by scaling of thermodynamic and transport processes*, *Am. J. Sci*., 307: p 861-900

Subtask 6.3 Compositional effects on BSR

Gas hydrate is often characterized in remote detection by seismic profiles and Bottom-Simulating Reflector (BSR), which is due to an abrupt acoustic impedance contrast between the base of gas hydrate stability zone (GHSZ) and free gas layer below. However, in some cases, hydrate is present but BSR is not observed. We hypothesize that multi-hydrocarbon components in a hydrate system can induce gradual transition of hydrate/free gas saturations, and result in a weak seismic reflection.

In last report, we have demonstrated that a small fraction of heavier hydrocarbon component can induce a gradual transition of hydrate/free gas saturations in sediment over a significant distance (relative to acoustic wavelength). If the thermogenic gas source from deeper sediment contains 5% (mol/mol) propane, a transition zone as thick as ~ 150 m can be formed, in which hydrate, gas, and aqueous phases can co-exist.

In this report, we will show that the saturation transition will cause a gradual transition of acoustic impedance. And seismic waves with different characteristic wavelengths are tested to find out the seismic response due to the transition zone.

1. An example saturation distribution of mixed-hydrate layers with a transition zone:

An example calculation of a CH_4-C_3H_8-H_2O System is presented in Fig. 6.3.1.

Here are the conditions and assumptions applied:

(1) Water-free propane molar fraction is 0.05 everywhere; Overall composition x_{CH4}=0.019, x_{C3H8}=0.001, x_{H2O}=0.98).

(2) Overall composition is the same in the spatial domain, (the fractionation of hydrocarbon components is neglected);

(3) Seafloor temperature T_{sf} = 276.15 K. Geothermal gradient G= 0.04 K/m.

(4) Seafloor Pressure P_{sf}=5 MPa.

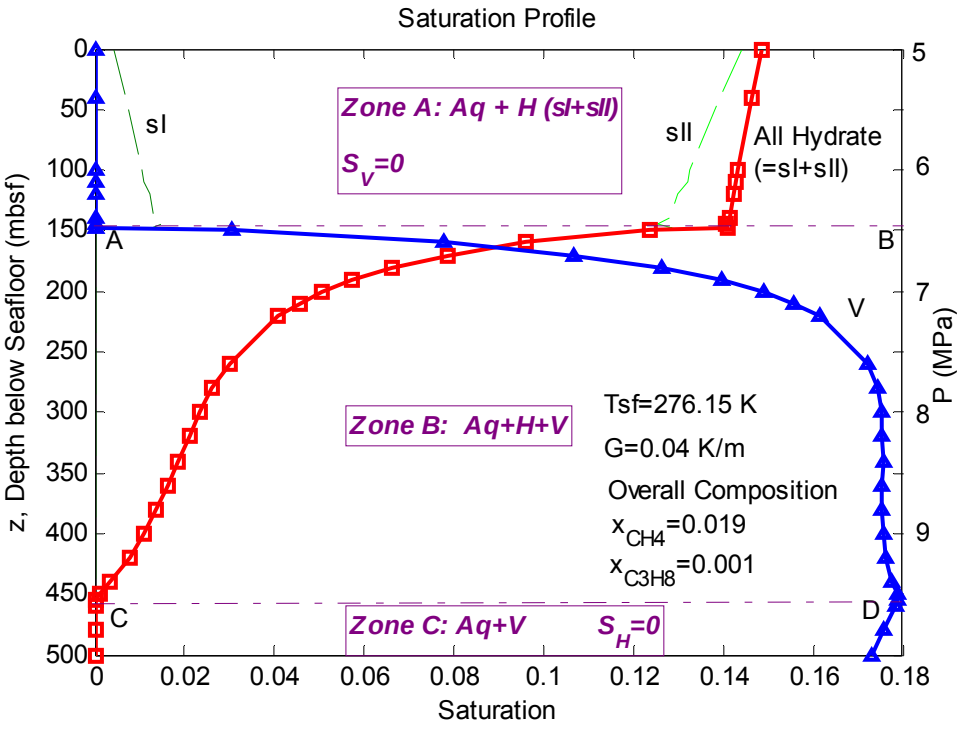

Fig. 6.3.1. Saturation Profiles for an example of mixed hydrate system

By using Sloan's program CSMGem v1.0 (Sloan, 2007), we obtained Fig.6.3.1. In this figure, for a CH_4-C_3H_8-H_2O System, in Zone B from z=147.5 mbsf (Line AB) to z= 450 mbsf (Line CD), the hydrate saturation, S_H, decreases continually from 14.1% to 0%, while vapor phase saturation S_V increases continuously from 0% to 17.9%. Zone B is a phase transition zone, in which 3 phases (Aq+H+V) co-exist, and saturations change continuously.

A gradual saturation change will result in the gradual change of acoustic properties with increase in depth, and consequently, very possibly induce a weak BSR, or even absence of BSR.

2. Acoustic Impedance Profile

Timur (Timur, 1968) suggested a Time-average equation, and Pearson (Pearson et al, 1983) applied that into hydrate system:

$$\frac{1}{V_p} = \frac{\phi(1-S_h)}{V_w} + \frac{\phi S_h}{V_h} + \frac{(1-\phi)}{V_m} \quad (6.3.1)$$

where V_p --- compression velocity of the hydrate layer;

V_h --- compression velocity of the pure hydrate;

V_w --- compression velocity of the fluid;

V_m --- compression velocity of the mineral;

ϕ --- porosity (as a fraction);

S_h --- Hydrate Saturation

When considering Vapor phase, suppose vapor phase can be treated with other phases like hydrate or liquid, then we can slightly adjust the above Equation-6.3.1 into:

$$\frac{1}{V_p} = \frac{\phi(1-S_h-S_v)}{V_w} + \frac{\phi S_h}{V_h} + \frac{(1-\phi)}{V_m} + \frac{\phi S_v}{V_v} \qquad (6.3.2)$$

The properties of each component are listed in Table 6.3.1.

Table 6.3.1. P-wave velocity and density of materials

component	V_p (m/s)	ρ (kg/m^3)
water	1500	1030
hydrate	3300	900
mineral	4370	2700
vapor	~400	~50*

*: an estimated value at the middle of steep transition zone, from Sloan's program, CSMGem v1.0. The mass of vapor phase occupies a very small fraction comparing to the mineral and water, hydrate, so its variation due to pressure and temperature change won't affect the estimated average density very much, therefore, we use an estimated value at a fixed *P,T* condition in the middle of the steep transition zone.

The average density of the sediment is estimated as:

$$\overline{\rho} = (1-\phi)\rho_{mnr} + \phi\sum_i S_i\rho_i \qquad (6.3.3)$$

where

$\overline{\rho}$ --- average density of the sediment

ρ_{mnr} --- density of mineral

S_i --- Saturation of phase *i* in pore space (i=water, vapor, hydrate)

ρ_i --- density of phase *i*

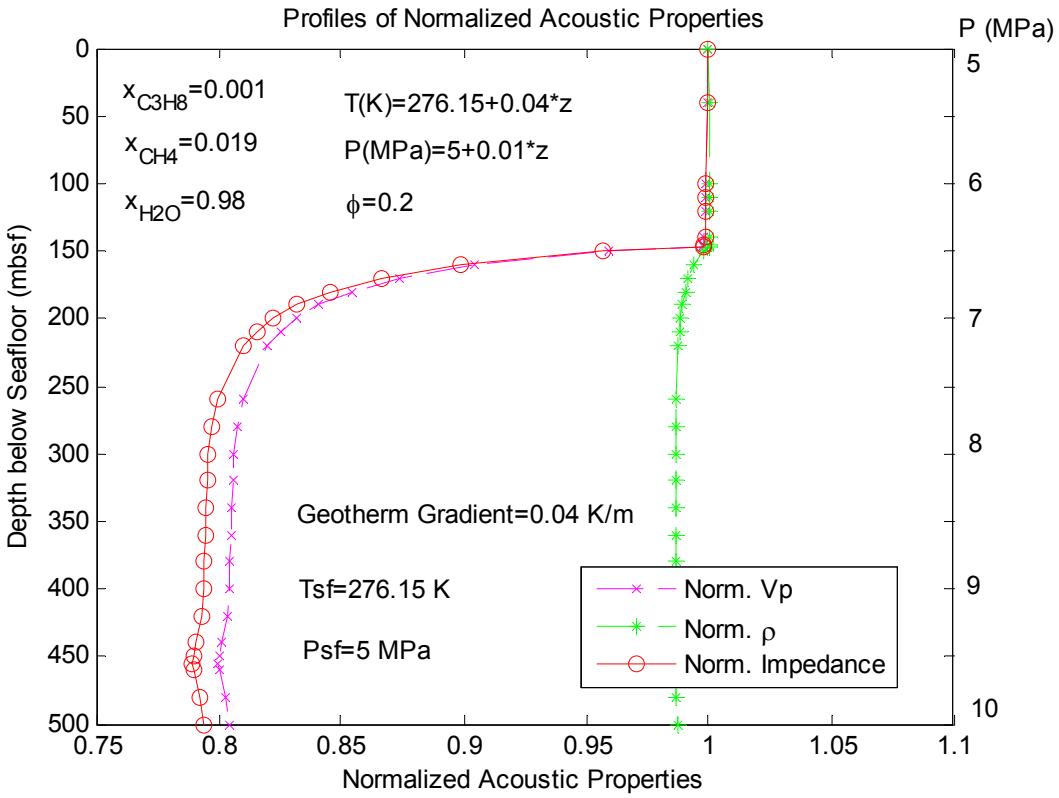

Fig. 6.3.2. Normalized Acoustic Property Profiles for an example of mixed hydrate system

Figure 6.3.2 is the acoustic property profiles, corresponding to the saturation profiles in Figure 6.3.1. All properties are normalized so that the values at seafloor are 1. Since the density varies very slightly (only around 2%), the velocity variation is the major cause of impedance variation. In later calculation, it's possible to assume that density is constant.

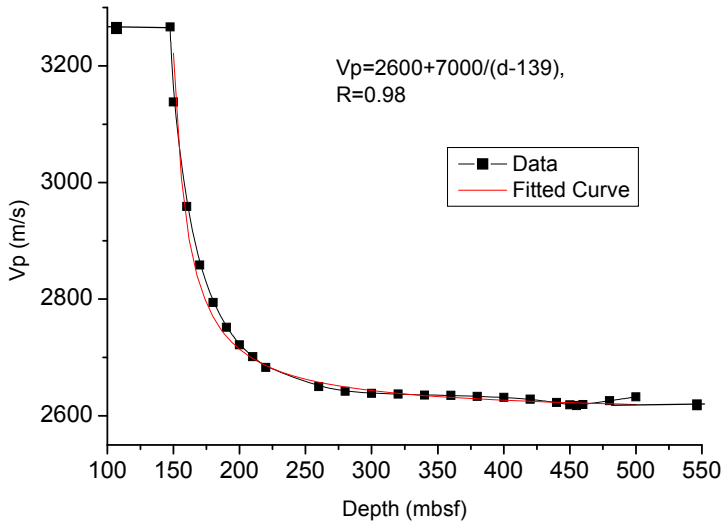

Fig. 6.3.3. Fitted Curve for the P-wave velocity V_p Profile

The (compressive) velocity profile in Fig. 6.3.2, can be approximated by using curve fitting in segment by segment, as shown in Fig. 6.3.3. The middle part can be fitted as:

$$V_p = A + B/(d - C) = 2600 + 7000/(d\text{-}139)$$

where A, B, C are constants. *d* is the depth below seafloor.

3. Seismic Response

In the detail of the velocity profile (Fig. 6.3.4), we may divide the whole transition zone into 2 types of segments: a steep transition zone, and a gradual one. The thickness of the whole transition zone is: $L_{Trans} = L_{SteepTrans} + L_{GradTrans}$. The steep transition zone is the zone, in which the velocity decreases very rapidly. In Fig. 6.3.4., $L_{SteepTrans} \approx 30$m, though the length of the whole transition zone is $L_{Trans} \approx$ 150m.

The rest is a gradual transition zone. The overall reflection is the effects of the whole transition zone, including steep transition zone and gradual one. The calculation has considered both types of segments. However, in the calculation, we find out that it's the steep transition zone that affects the response most greatly, because the gradual transition zone tends to induce weak reflection. That's why we need to find an appropriate characteristic length $L_{SteepTrans}$, instead of L_{Trans}.

Therefore, for characterization purpose, the ratio of maximum wavelength, to the thickness of the Steep Transition Zone, $\lambda_{\max} / L_{SteepTrans}$, may be used instead of the $\lambda_{\max} / L_{Trans}$, to characterize the seismic response.

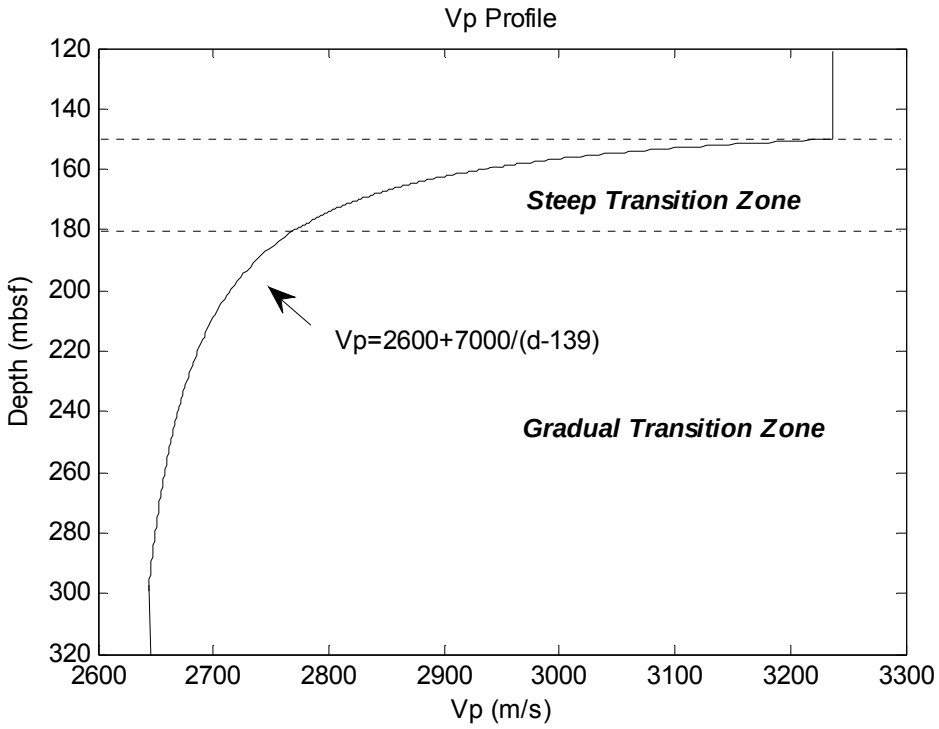

Fig. 6.3.4. Detail in the V_p Profile

To calculate the seismic response, a source function with a finite bandwidth is used as the source signal. It's defined in time domain as:

$$f(t) = \frac{1}{2\pi(a-b)}\left[\frac{\sin(2\pi at)}{t} - \frac{\sin(2\pi bt)}{t}\right]$$

Frequency band: *a, b* are parameters (Hz). The denominator $2\pi(a-b)$ is just for normalization. We set *a=3b* to avoid ringing waves. The FFT of an example ource signal with bandwidth of *b~a* Hz is plotted in Fig. 6.3.5.

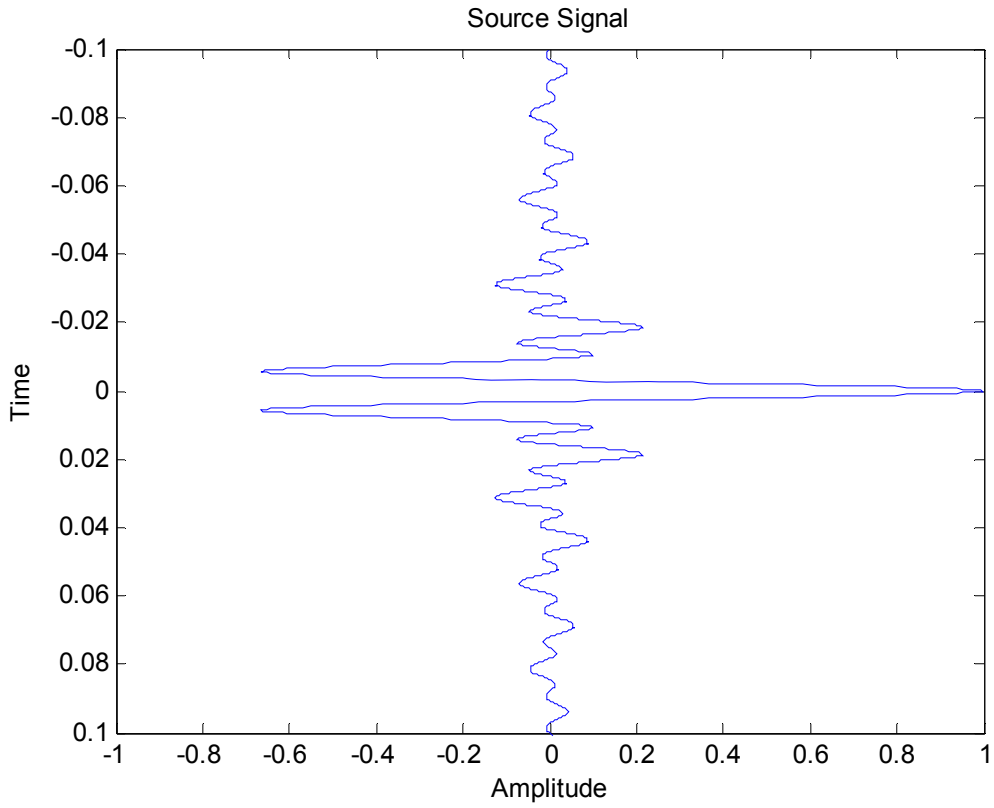

Fig. 6.3.5a. An example source signal, in time domain. Amplitude of peak wave is A_0=1.0. For this figure, the bandwidth is [40, 120] Hz.

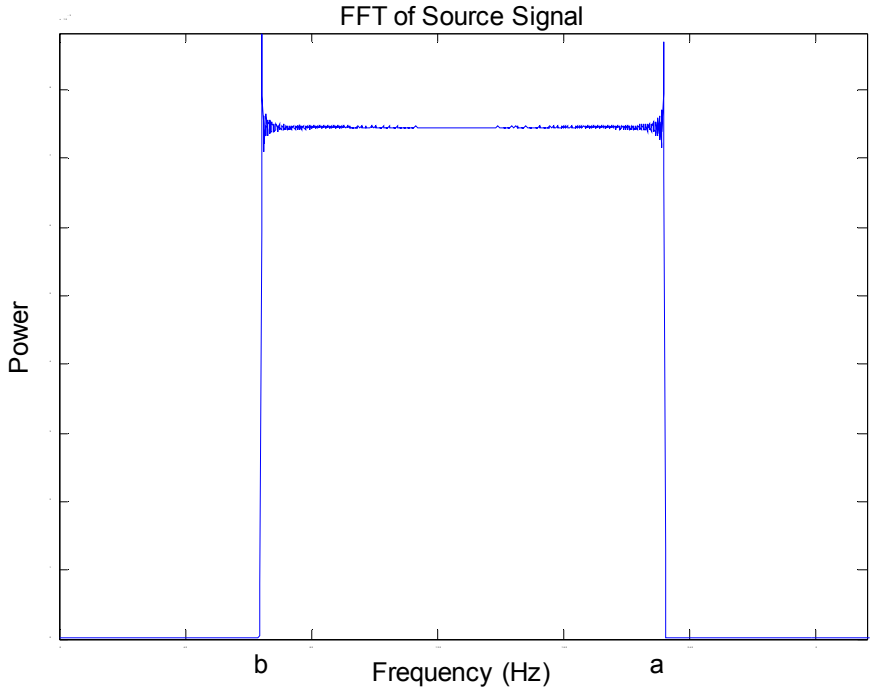

Fig. 6.3.5b. FFT of the Source Signal (*a*=3*b*)

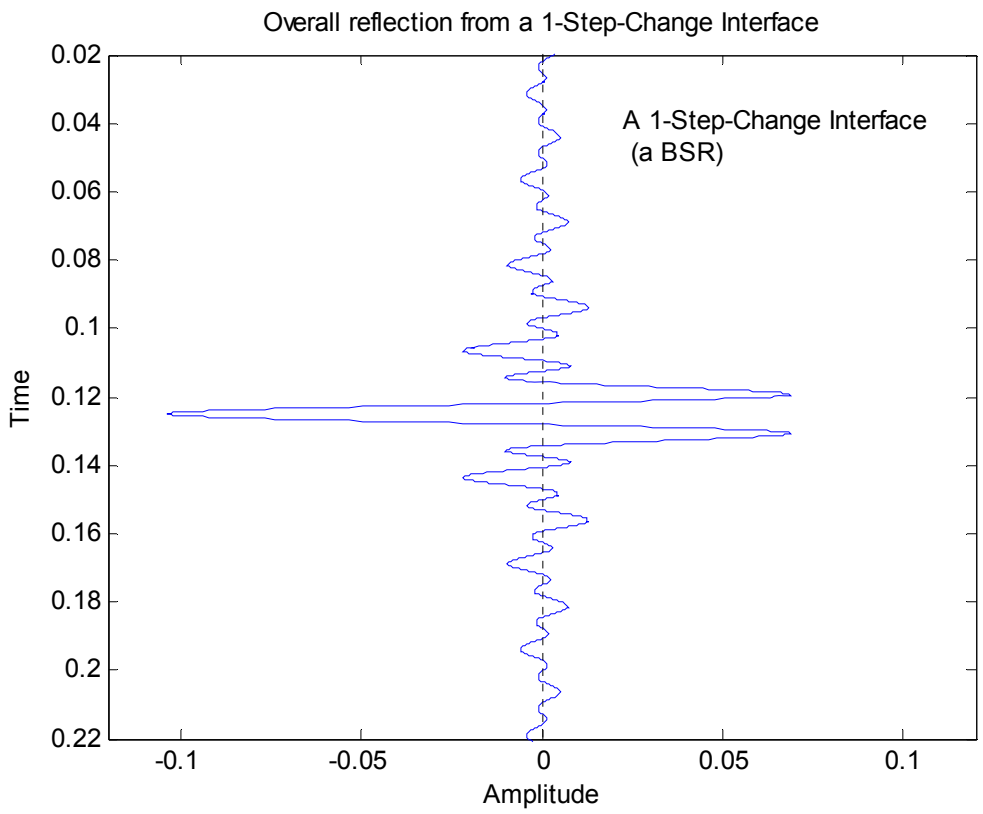

Fig. 6.3.5c. Reflection from A 1-Step-Change Interface (i.e., a sharp transition, or a BSR). The starting and ending velocities are the same as in Fig. 6.3.4. The amplitude of peak wave is $A_{BSR}=0.103A_0$, where A_0 is the amplitude of the source signal in Fig.6.3.5a. Bandwidth: [40, 120]Hz.

Assume a 1-D plane wave is distributed into the sediment, and the reflections by the sediment layers are calculated. Assume the sediment can be approximated by a number of thin layers. If there is only a 1-step-change interface, just like a BSR (which is a sharp transition zone with infinitesimal thin thickness) in the methane hydrate system, then the reflection is shown as Fig. 6.3.5c.

Source signals of the same type as shown in Fig. 6.3.5, with a series of bandwidths, e.g., [5, 15]Hz, [10, 30]Hz, … [80, 240]Hz are used to test the response, when considering a mixed-hydrate system in which a thick transition zone exists. The result is different from a BSR response (Fig. 6.3.5c).

In the mixed-hydrate case, the whole transition zone was discretized into 300 layers. The steep transition zone, which is only around 30 m, was specially discretized into 200 layers to avoid numerical distortion, because the change of impedance in this layer is very rapid along the depth direction. The result is shown in Fig. 6.3.6.

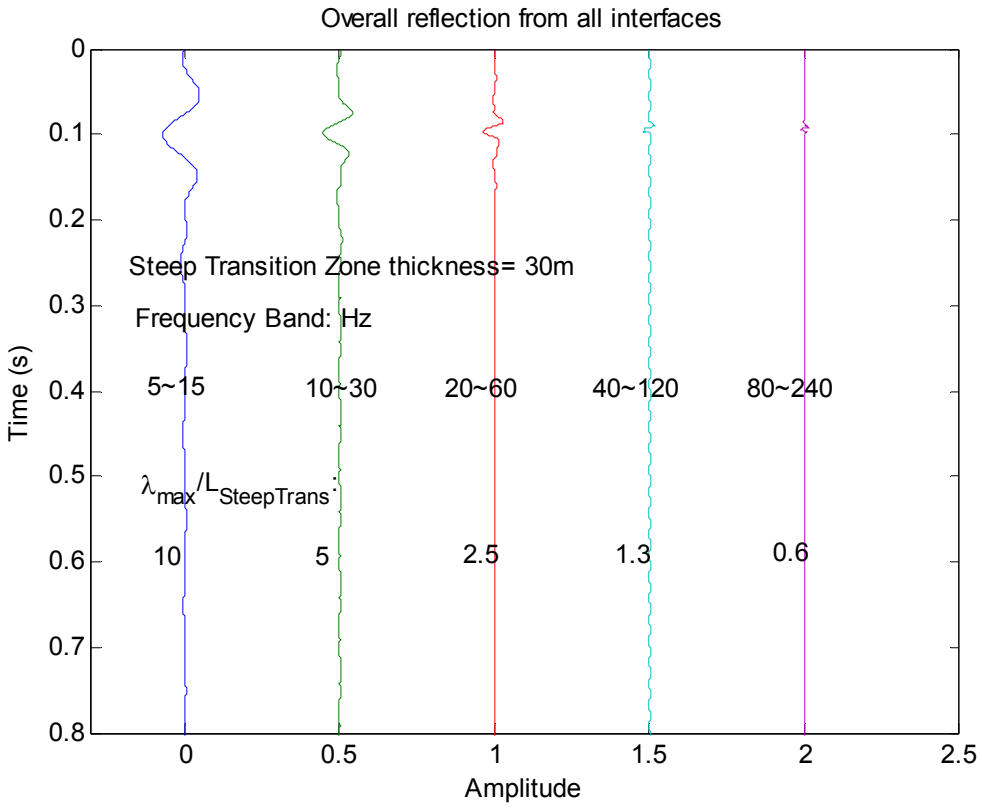

Fig. 6.3.6. Response for waves with different wavelengths

By comparing the amplitude of the peak of reflection signal A, with A_{BSR}, if A/A_{BSR} is in the order of O(1), then we consider this as a strong reflection; if it's in the order of O(0.1), or less than O(0.1), then it's considered as a weak reflection. From Fig. 6.3.6, it's observed that:

If $\lambda_{\max} / L_{SteepTrans}$ < 1, reflection is weak.

If $\lambda_{\max} / L_{SteepTrans}$ > 5, reflection is strong.

Once again, the calculation has considered the whole transition zone, including both steep and gradual ones. However, it's the steep transition zone that affects the response most greatly, because gradual zone(s) tends to induce weak response. That's why we need to find an appropriate characteristic length $L_{SteepTrans}$, instead of L_{Trans}

4. Conclusion

The seismic reflection from a mixed hydrate system has been calculated. It indicates that, in a mixed hydrate system, a thick transition zone may appear. A Steep Transition Zone is chosen to characterized the zone in which velocity varies very rapidly. A parameter, $\lambda_{\max} / L_{SteepTrans}$, the ratio of maximum wavelength, to the thickness of the Steep Transition Zone, is used to characterize the seismic response.

It's shown that, if $\lambda_{\max} / L_{SteepTrans}$ is less than 1.0, then the reflection may be very weak; but if it's larger than 5, the reflection might be very strong.

Admittedly, the boundaries of the steep transition zone needs more discussion.

This indicates that in the case of a multi-hydrocarbon hydrate system, the reflection response is dependent on the thickness of (steep) transition zone and seismic wavelength. This provides a possible mechanism why in some places hydrate is present but BSR is not observed.

Reference:

1. Sloan, E.D. and Koh, C. A., *Clathrate Hydrates of Natural Gases*. 3rd ed. 2007: CRC Press.
2. Sloan, E.D. and Koh, C. A., CSMGem v1.0, 2007.
3. Pearson, C.F., J. Murphy, and R. Hermes, *Acoustic and resistivity measurements on rock samples containing tetrahydrofuran hydrates: Laboratory analogues to natural gas hydrate deposits.* J. Geophys. Res., 1986. **91**: p. 6.
4. Timur, A., *Velocity of Compressional Waves in Porous Media at Permafrost Temperatures.* Geophysics, 1968. **33**(4): p. 584.

Task 7: Analysis of Production Strategy

J. Phirani & K. K. Mohanty, University of Houston

Introduction

In this work, gas production from unconfined class 2 hydrate reservoirs is studied and pore scale modeling is used to estimate transport properties of hydrate bearing sediments. In our previous work, we had studied warm water flooding of **confined** class 2 hydrate reservoirs. For confined reservoirs, if the production pressure is low, depressurization is better than warm water injection. If the production pressure is not very low, injection of warm water is preferable. At high injection temperature, gas production rate increases with injection pressure. The current work is focused on unconfined hydrate reservoirs. Different temperatures and pressures for injection and production wells are considered to optimize gas production from unconfined reservoirs.

Hydrates in the geological settings are formed by methane saturated water moving up from warmer regions to colder regions in the hydrate stable zone. Hydrates deposit on the walls of pore; effective porosity and permeability of the formation decreases as the hydrate saturation increases. In the present simulator, the effective porosity decreases as the hydrate saturation increases and permeability is a function of the effective porosity. The relative permeability is a function of effective saturation of the fluid phases. In this study, we use pore-scale modeling (percolation theory) to find these transport properties as a function of hydrate saturation.

Methodology

The objective of this study is to identify optimum production strategies for gas production from unconfined Class 2 hydrate reservoirs through numerical simulation. The domain selected as the base case is a quarter five-spot of size 120m x120m x11m (Figure 1). Initial temperature and pressure are assumed to be 7.5°C and 9MPa at the bottom of reservoir, respectively, which lie in the hydrate stable zone. The initial temperature varies with a geothermal gradient of 0.03C/m and pressure as hydrostatic gradient of water. The bottom 3m of the domain is an aquifer layer (S_A=1.0) and the top 8m is a hydrate layer with a hydrate saturation, S_H of 0.6 and aqueous saturation, S_A of 0.4. There is no heat and mass transfer though the side boundaries due to symmetry. There is only heat transfer, but no mass flow through the top boundary. For the case of unconfined aquifer, a constant pressure boundary is considered for the bottom surface and water can come into the reservoir or go out of the reservoir depending on the pressure at a particular time step. The bottom 1 meter of the reservoir is given a low permeability (1/10th of the permeability of reservoir) to

constrain the water flow to and from the aquifer. The effect of injection temperature, injection pressure and production well pressure on gas and water production is studied. The saturation histories encountered in these simulations will be modeled at the pore scale for transport properties.

The numerical model used is a finite-volume simulator that takes into account heat transfer, multiphase fluid flow and equilibrium thermodynamics of hydrates. Four components (hydrate, methane, water and salt) and five phases (hydrate, gas, aqueous-phase, ice and salt precipitate) are considered in the simulator. Water freezing and ice melting are tracked with primary variable switch method (PVSM) by assuming equilibrium phase transition. Equilibrium simulation method is used here because kinetics of hydrate formation and dissociation are relatively fast in the field-scale. This in-house simulator has been validated in the DOE code comparison study.

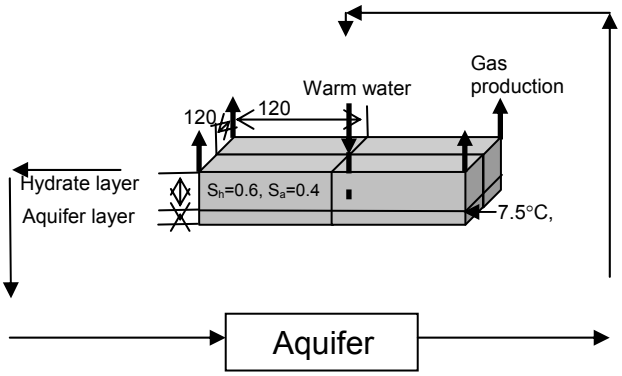

Figure 1: Domain considered for the base case

For pore-scale modeling, hydrate deposition in a single pore was estimated using the 3-D simulator for different pore radii to find the dependence of hydrate deposition rate in a pore on the pore radius. Hydrates deposit on the pore walls and thickness of hydrate layer is found to be independent of the pore size until the pore is plugged. Percolation theory is used to find the transport properties. The initial pore size distribution was assumed to follow a Rayleigh distribution. The pore size distribution is recalculated after depositing a given hydrate saturation.

Results

Methane production was simulated for different injection pressures, injection temperatures and production pressures for 3000 days and total production of gas was compared for these parameters.

Figure 2 shows the production curves for different injection and production pressures. For injection cases, the temperature of the warm water has been fixed at 50C. The cumulative gas production increases with increasing injection pressure. The lowest production is in the case of no injection. Depressurization pressure has been varied from 2 MPa to 4 MPa; it does not affect the total production significantly. The production curves for different depressurization pressure are close if the injection pressure is same. The 2MPa depressurization pressure has a slight higher production. The depressurization alone does not help in hydrate dissociation because the water from the infinite aquifer does not allow the pressure to go below the initial pressure in the reservoir except in the near-well regions. Hydrates dissociate only in the region near the depressurization well. The warm water flooding at a temperature of 50C increases the cumulative production. Even warm water injection at an injection pressure of 20MPa increases the cumulative gas production significantly more than the no injection case. With the increasing injection pressure, the production of gas increases. More heat is supplied to the formation which dissociates more gas. However, a part of the injected warm water goes into the infinite aquifer and that extra heat is not used for hydrate dissociation.

Figure 3 shows the pressure profile along the plane connecting injection and production wells for the case the production pressure is 2MPa and injection pressure is 30MPa. Warm water is injected at 50C. Most of the pressure drop is in the near-well region only.

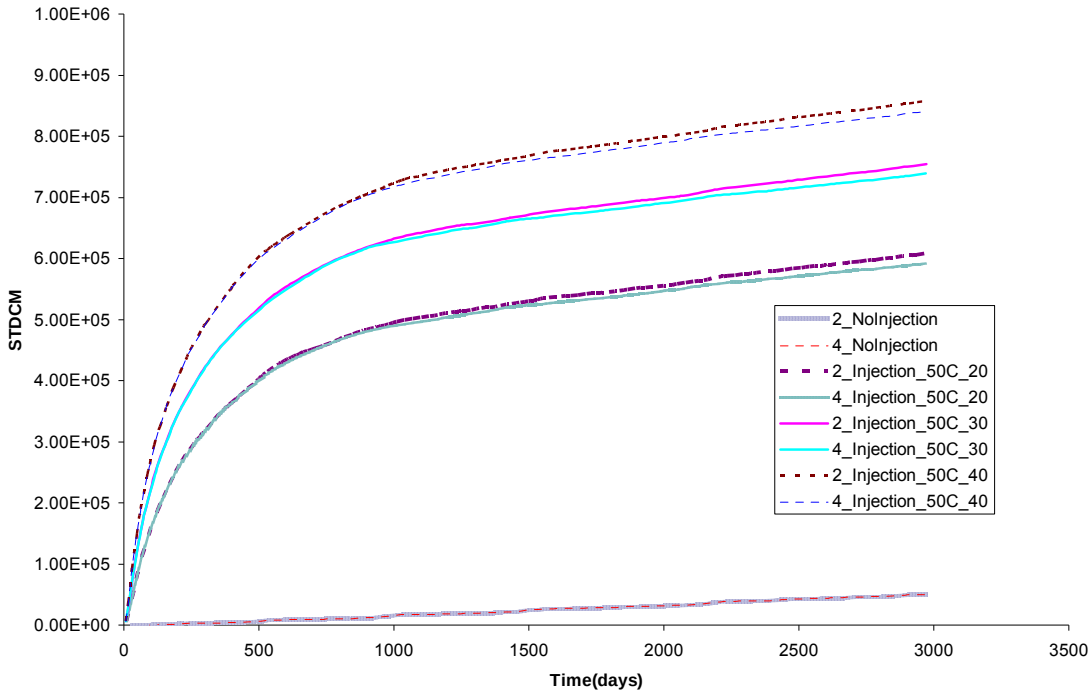

Figure 2: Cumulative production for different injection pressure for unconfined reservoir

Figure 4 shows the in-situ hydrate saturation profile along the same plane. The hydrate dissociation is mostly near the injection well because of the increase in temperature. The pressure decrease is confined to the region near the production well and hence only a small amount of hydrate dissociates in that region. The hydrate saturation downstream of the dissociation front is higher than the initial hydrate saturation. The gas produced at the dissociation front recombines with the water to form hydrates. This reduces the permeability decreasing the convection of warm water in horizontal direction.

To find the optimum injection temperature, we keep the injection pressure constant at 20MPa for different injection temperatures. The production pressure is 4MPa. Figure 5 shows the production curve for these cases. From no injection to 20C injection at 20MPa pressure, the cumulative gas production increases significantly. With increasing temperature, the cumulative gas production also increases. But beyond 30C, there is not much increase in cumulative production for each 10C rise in temperature of injection water. This is due to the infinite aquifer which after some time takes most of the injected water and heat does not reach the hydrate for dissociation. So, increasing the temperature beyond 30C does not help much in increasing the gas production by a large amount.

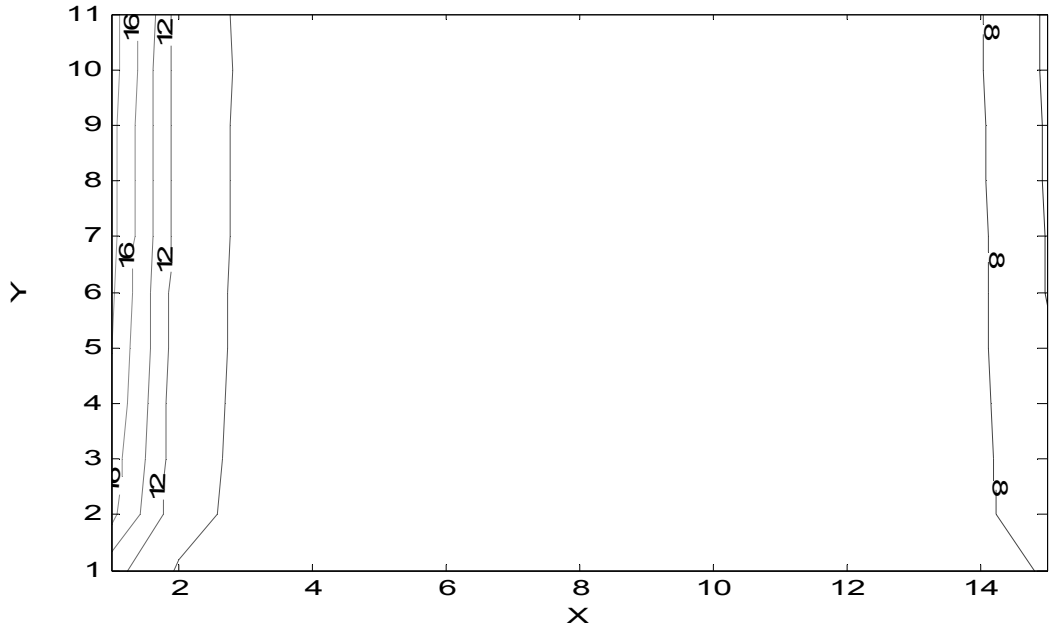

Figure 3: Pressure profile after 3000 days in an unconfined reservoir with for injection pressure 30MPa, injection temperature 50C and production pressure 2MPa.

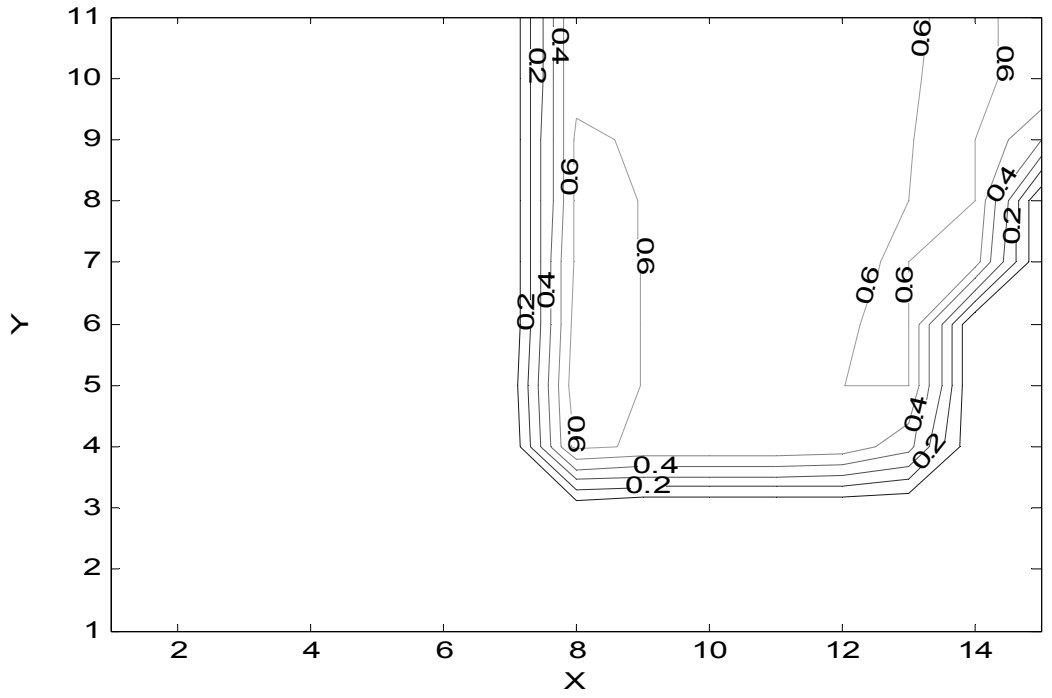

Figure 4: Hydrate saturation profile after 3000 days in an unconfined reservoir with for injection pressure 30MPa, injection temperature 50C and production pressure 2MPa.

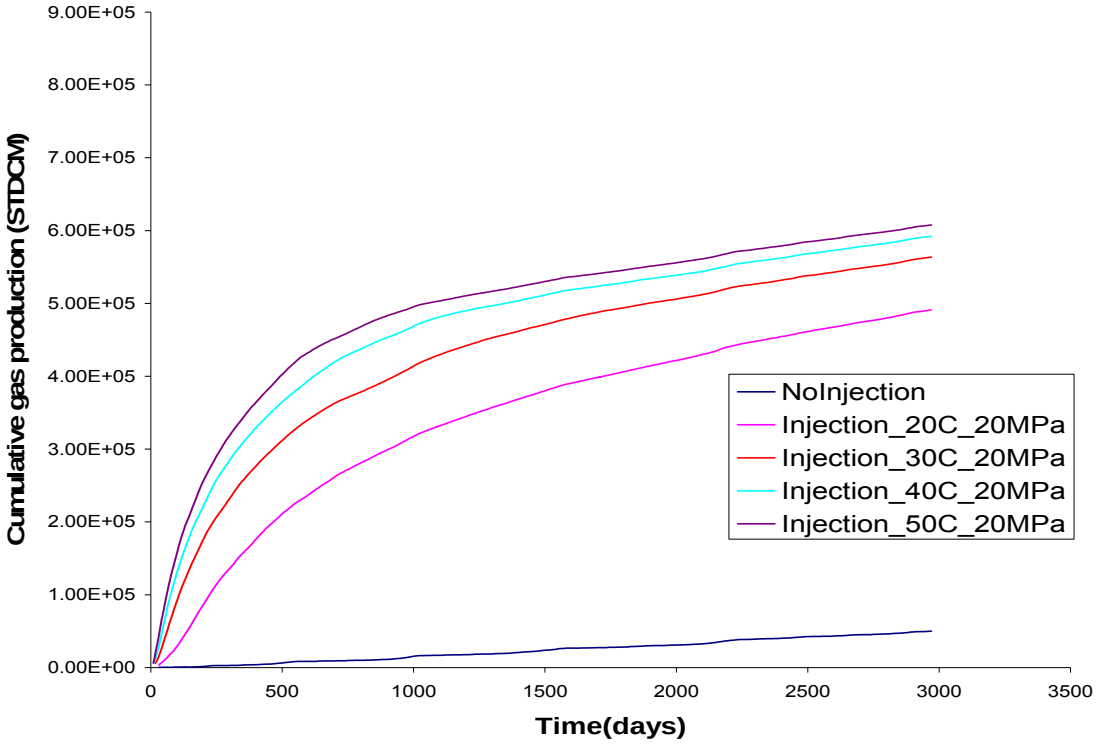

Figure 5: Cumulative gas production for different injection temperature at 20MPa injection pressure and 4MPa production pressure.

Figure 6 shows the permeability for different hydrate saturations and a quadratic fit for the curve from pore-scale modeling. It compares the permeability obtained by Civan's power law model and the permeability estimated using percolation theory for different hydrate saturations. Civan (2001) power law model is stated as:

$$\frac{K^e}{K_0} = \frac{\phi}{\phi_0}\left(\frac{\phi^e(1-\phi_0)}{\phi_0(1-\phi^e)}\right)^{2\beta},$$

where K^e is the effective permeability, K_0 is the reference permeability which is taken as 0.017708 darcy at reference porosity ϕ_0 0.25. The absolute permeability K, changes with ϕ according to the above equation with ϕ_e equal to ϕ. For the present case ϕ is always equal to ϕ_0 because of homogeneity. ϕ^e is the effective porosity for the fluid phases which can be related to absolute porosity, ϕ as:

$$\phi^e = \phi(S_G + S_A) \ .$$

The permeability estimated from the two models are very different. The models should be verified with experimental results for their validity.

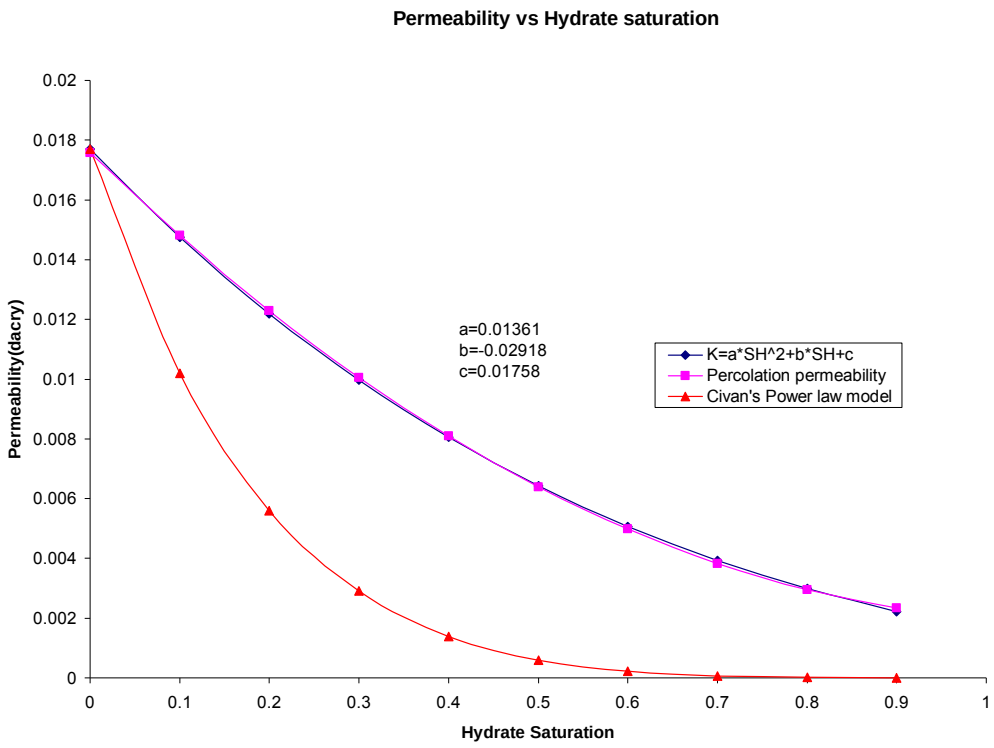

Figure 1: Permeability for different hydrate saturations.

Conclusions

Depressurization in the unconfined reservoir is ineffective. Thermal stimulation is necessary for gas production. The low temperature of 20C of injection water helps in thermal stimulation of hydrate reservoirs. Increase in injection temperature and pressure increases gas production rate. The effective permeability estimated from the pore scale model is significantly higher than the Civan model often used in the literature.

Future Work

Only horizontal hydrate reservoirs have been studied so far; in future we would study dipping reservoirs. The reservoir described in this report has an infinite aquifer which always keeps the pressure constant. In the past, we have studied confined reservoirs, where the volume of the aquifer is of the order of reservoir volume. The reservoir in-between these two extreme cases need to be studied.

Pore scale modeling will be used to find relative permeability of the wetting phase (water) and the non-wetting phase (gas) for drainage and imbibition for different hydrate saturation. The results will be incorporated in the present simulator and production simulation will be done for production strategies of gas hydrates.

Task 8: Seafloor and Borehole Stability

Summary

We are moving forward on Task 8 as scheduled. We have begun integrating the sediment properties work (this task) with the geologic hydrate accumulation modeling (Task 6) by looking at how permeability and permeability anisotropy can be characterized over geologic time-scales and then incorporated in accumulation models. We are also assessing strength and pressure of sediment proposed for DOE-sponsored JIP hydrate work in the Gulf of Mexico; ultimately we are helping to develop a safe drilling program that will maximize our understanding of hydrate in the Gulf of Mexico and proved data for modeling these accumulations. We have also measured permeability to evaluate new techniques for estimating permeability anisotropy and getting robust permeability data from logging measurements.

Subtask 8.1: Sediment-Hydrate Properties

Overview

We have expanded our laboratory techniques to increase our understanding of permeability in sediments that can host hydrate. These baseline experiments will provide required for inputs to models that modify baseline permeability as a function of hydrate and/or gas saturation (e.g., Task 6, Task 7, Tough+Hydrate). We are also starting an experimental and theoretical program to look at the evolution of permeability anisotropy, which has been shown to be important on the geologic accumulation of hydrate (e.g. Task 6). Experiments are being performed on sediments from hydrate regions and on synthetic sediment mixtures.

Approach

We have added two new capabilities to the physical properties laboratory: (1) dead-weight consolidation; and (2) specific surface measurement for fine-grained sediments. With the dead-weight consolidation system we can use natural sediments of a known mineralogy or controlled mixtures of fixed grain size and mineralogy and control the maximum stress level applied to the sample. We have designed a suite of experiments with this equipment to look at permeability evolution and permeability anisotropy in sediments representative of marine hydrate settings (e.g., Gulf of Mexico; Cascadia, Nankai trough). We have materials directly from the Gulf of Mexico and Nankai trough for use. This consolidation approach will help us constrain the controls on fluid migration through numerical models which can be tested against field data. The specific surface measurements are being used with permeability experiments and log data from Keathley Canyon (Gulf of Mexico JIP) to help understand how

mineralogy affects flow properties and how log data can be best used to evaluation flow properties of fine-grained sediments.

Results and Discussion

Our experiments have just begun so we do not have any results at this stage. The theoretical work is promising as we are making linkages between pore throat flow models and log data (e.g. Kozeny-Carmen, NMR-permeability) that allow us to expand them from sand-sized reservoir systems to fine-grained seal and source regions. Continued experiments including permeability and NMR work will wrap up this phase of our permeability work. After that we will focus more on strength of sediments to better understand slope stability.

Subtask 8.2: Modeling (In)stability

Overview

We are using standard stability analyses for sediments to understand the evolution of stable and unstable conditions in marine sediments without hydrate, as hydrate accumulates, as hydrate dissociates, and as gas is produced from hydrate. This work will help us better understand large scale failures associated with hydrates as well as potential production-related hazards. The stability models will be integrated with our geologic and production models (Tasks 6 and 7). The equations have been tested in water-saturated systems and are being incorporated in our hydrate models.

Approach

Our basin-scale models of fluid flow have been coupled to a slope stability calculation that were tested in the absence of hydrate. These models have been validated and are being included in the hydrate models (beginning with Task 6). Currently we have limited data on cohesion and friction angle of sediments with hydrate so we have limited constraints to test the models. The first test will be a hydrate-free model (in the geologic hydrate model) which can be tested against our water-phase model. We then will explore frictional strength and cohesion which should change as a function of saturation (water, gas, hydrate) and lithology (sand, silt, clay). Sensitivity studies and parameter tests will be critical to this portion of the research as we try to isolate the key driving forces for unstable conditions.

Subtask 8.3: Integrating geomechanical studies

Overview

This subtask involves assessing ongoing geomechanical studies to maximize our understanding of geomechanical properties of hydrate bearing sediments across

DOE-funded projects. The goal is a comprehensive geomechanical database and modeling approach with a means to understand these properties at geologic and human time-scales. We have worked directly with the USGS, MIT, GATech, and LBNL compile a manuscript that should be submitted in November, 2008.

Waite, W., Santamarina, C., Cortes, D., Dugan, B., Espinoza, N., Germaine, J., Jang, J., Jung, J., Kneafsey, T., Shin, H., Soga, K., Winters, W., Yun, T-S., in prep, Physical Properties of Hydrate-Bearing Sediments, Reviews of Geophysics.

Hydrate Presentations

July 2008 Lunch and Learn Seminar at Shell International Exploration and Production Inc. entitled "Geologic Accumulation of Hydrates in Marine Sediments." The talk was an overview presentation on the DOE-sponsored hydrate project at Rice University (Dugan).

July 2008 Rice University Consortium on Processes in Porous Media – presentation on NMR permeability estimation in hydrate systems (Daigle).

Hydrate Activities

DOE/IODP Hydrate Drilling [Aug 2008 – present] – Dugan has been working on evaluation of hydrate-related drilling hazards in the Gulf of Mexico and how existing and new drilling techniques could be used to facilitate DOE/JIP drilling of hydrate in the Gulf with the IODP drillship

DOE/JIP Site Selection Working Group member [2007-present]

Geofluids Editorial Board member [2007-present]

Publications

Daigle, H., Dugan, B., in review, Extending NMR Data for Permeability Estimation in Fine-Grained Sediments, Marine and Petroleum Geology.

Dugan, B., 2008, Fluid Flow in the Keathley Canyon 151 Mini-Basin, Northern Gulf of Mexico, Marine and Petroleum Geology, 25(9), 919-923, doi:10.1016/j.marpetgeo.2007.12.005.

Hutchinson, D.R., Hart, P.E., Ruppel, C.D., Snyder, F. and Dugan, B., in press, Seismic and thermal characterization of a Bottom Simulating Reflection in the northern Gulf of Mexico, in Collett, T.S., Johnson, A., Knapp, C., Boswell, R. (Eds.), Natural Gas Hydrates: Energy Resources, Potential and Associated Geologic Hazards. AAPG Special Publication.

Winters, W.J., B. Dugan, T.S. Collett, 2008, Physical Properties of Sediments

from Keathley Canyon and Atwater Valley, JIP Gulf of Mexico Gas Hydrate Drilling Program, Marine and Petroleum Geology, 25(9), 896-905, doi:10.1016/j.marpetgeo.2008.01.018.

Abstracts/Conference Proceedings

Bhatnagar, G., Chapman, W.G., Dickens, G.R., Dugan, B., Hirasaki, G.J, 2008, Effects of Overpressure on Gas Hydrate Distribution, Sixth International Conference on Gas Hydrates, Vancouver, British Columbia, Canada.

Bhatnagar, G., Chapman, W.G., Dickens, G.R., Dugan, B., Hirasaki, G.J, 2008, Relating Gas Hydrate Saturation to Depth of Sulfate-Methane Transition, Sixth International Conference on Gas Hydrates, Vancouver, British Columbia, Canada.

Chatterjee, S., Bhatnagar, G., Chapman, W.G., Dickens, G.R., Dugan, B., Hirasaki, G.J., 2008, Effect of Lithologic Heterogeneities on Gas Hydrate Distribution, AGU 2008 fall meeting, San Francisco, CA.

Daigle, H.C., Dugan, B., 2008, Extending Nuclear Magnetic Resonance Data for Permeability Estimation in Fine-Grained Sediments, AGU 2008 fall meeting, San Francisco, CA.

Hustoft, S., Dugan, B., Mienert, J., 2008, Integrated Hydrological Flow-Modeling and 3D Seismic Analysis of the Nyegga Pockmark-Field at the Mid-Norwegian Constrain Times of Methane Leakage, Subsurface Sediment Remobilization and Fluid Flow in Sedimentary Basins Conference (The Geological Society), 21-22 October 2008, London, England.

Task 9: Geophysical Imaging of Gas Hydrate and Free Gas Accumulations

For this task in particular, and others in general, we have successfully initiated collaboration with National Institute of Oceanography (NIO), India. We intend to demonstrate geophysical imaging with multichannel seismic data from the Krishna-Godavari (K-G) basin in the Indian east coast. NIO scientist, Dr. Pawan Dewangan, visited Rice University in the last week of July. During his visit Pawan presented examples highlighting the variations in the hydrate content. An interesting example is a case of three wells, 10, 12 and 13 (Figure 1), drilled within 500 m range of each other that show rapidly varying hydrate concentration. While Well 10 encountered 128 m of hydrates, Well 12 and 13 encountered less than 60 m of massive hydrates. It was mutually agreed that modeling of the seismic line that is closest to these three well will be undertaken.

Priyank Jaiswal, now a post-doctoral research associate at Rice University, started working on the gas hydrate project officially, from September 15, 2008. Priyank traveled to NIO on September 29 and has been working on subtask 9.1 since then.

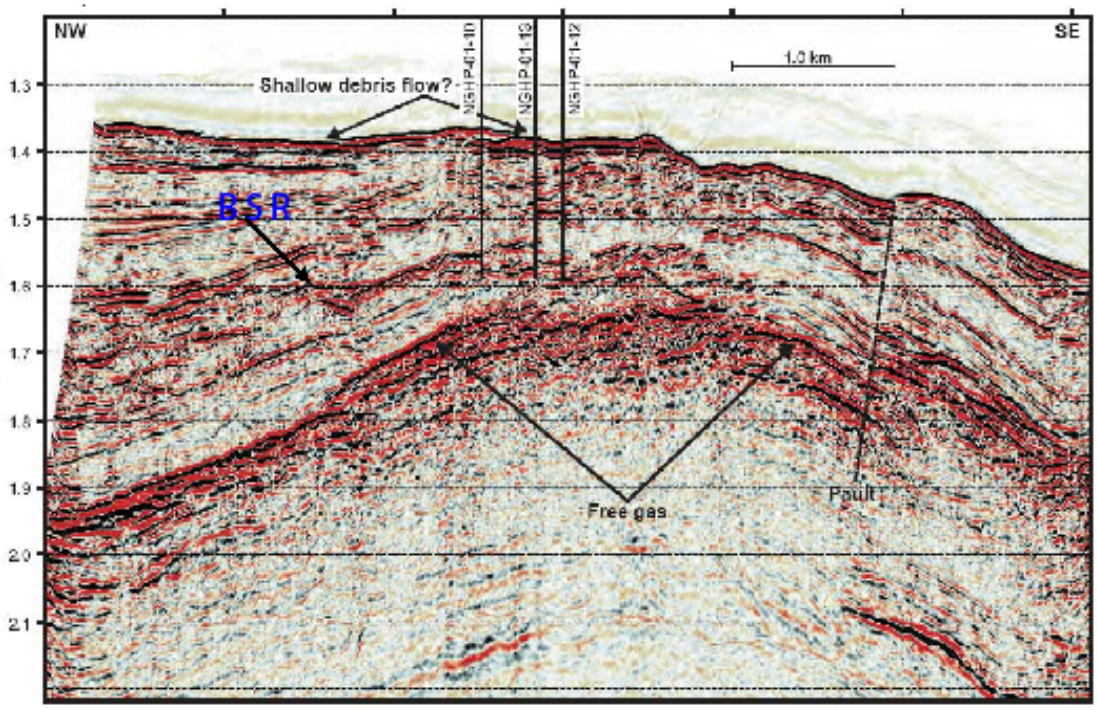

Figure 9.1. Seismic line and wells. While Well 10 (left) found ~128 m of massive hydrates, Well 13 (center) and Well 12 (right) found less than 60 m of hydrate rich zones. Log data from Well 10 is ready to be used in conjunction with seismic data. Data from Well 12 and 13 are currently being processed at NIO. The seismic line is as a result of previous processing from NIO in 2007.

Subtask 9.1: Preliminary processing and inversion of seismic data.

The seismic line under investigation comprises of ~600 shot gathers with shot and receiver spacing of 12.5 m and a nominal fold of 60. The minimum and maximum source-receiver offsets are 70m and 1570m. The seafloor depth varies from 1040 - 1200m depth in the study area. The depth of investigation is within 300m of the seafloor.

A bulk of our effort so far has gone in applying static shift to the data such that the seafloor primary and multiple are aligned and the sea-floor reflection is coherent. The next steps in processing, that have led to the creation of stack (Figure 9.2) are as follows:

a) Deconvolution (Yilmaz 2001). It was mainly aimed at removal of bubble effect. Careful deconvolution with several sets of free parameters such as gate sizes and autocorrelation lengths have indicated that a reflector that was previously (prior to collaboration with Rice) being interpreted as base of debris flow (Figure 9.1) was an artifact. The presence or absence of shallow debris flow will have an overall impact in understanding of the geomorphological features in the study area.
b) Butterworth bandpass filtering (3-6-40-80Hz), followed by F-K filtering to remove low-frequency linear noise trains (most likely related to acquisition), and F-X filtering to increase coherency of reflection events. No effort was made to remove multiples as the zone of interest lies within the first multiple.
c) Velocity analysis. The data were sorted in the common mid-point domain and used for the stacking velocity analysis till the deepest stratigraphy of interest (a reflector below the interpreted BSR at 1.7s two-way-time in the center of the image). Stacking velocity analysis is done in an iterative manner where each iteration comprises of velocity picking followed by normal move-out (NMO) and dip move-out (DMO; Hale 1984) corrections, followed by the inverse NMO corrections and re-picking of the velocities. Velocity picking was iteratively conducted till two subsequent stacking velocity models were found to have minimal differences; at this stage the data were stacked after NMO and DMO corrections. The velocity model from the stacking velocity analysis is used for stacking the data and is also transformed to an interval velocity model which in turn used for both time and depth migration using Kirchoff Pre-Stack method (PSDM; Schneider 1978). After the first iteration of velocity analysis, true amplitude recovery was also applied.

d) PSDM. The velocities from velocity analysis above were converted to interval velocities and used for PSDM using the common offset section prepared for DMO.

Figure 9.3 is the LWD log from Well 10. The BSR appears to be at 160m depth below the seafloor. Figure 9.4 is the PSDM image using. The figure suggests that the image is in agreement with the log. Due to limited source-receiver offsets (1.57 km), velocities below 1.6s determined by stacking velocity analysis have larger associated uncertainties.

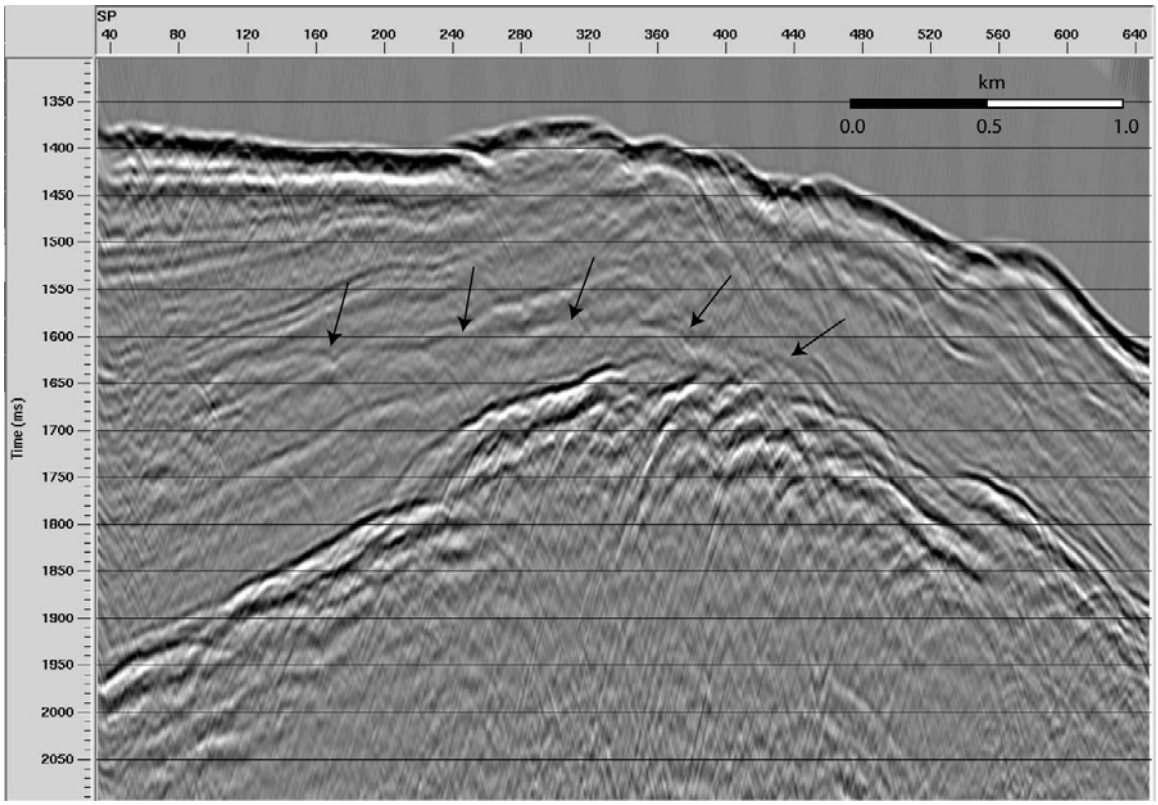

Figure 9.2 Stack data. BSR is indicated with black arrows. Between CDPs 480 and 600, BSR is not interpretable.

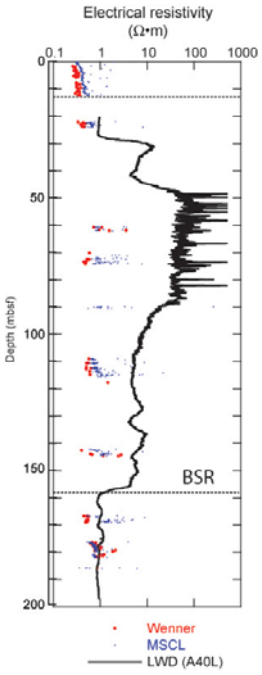

Figure 9.3 LWD log from well 10. The BSR is interpreted at ~160m depth from the sea floor.

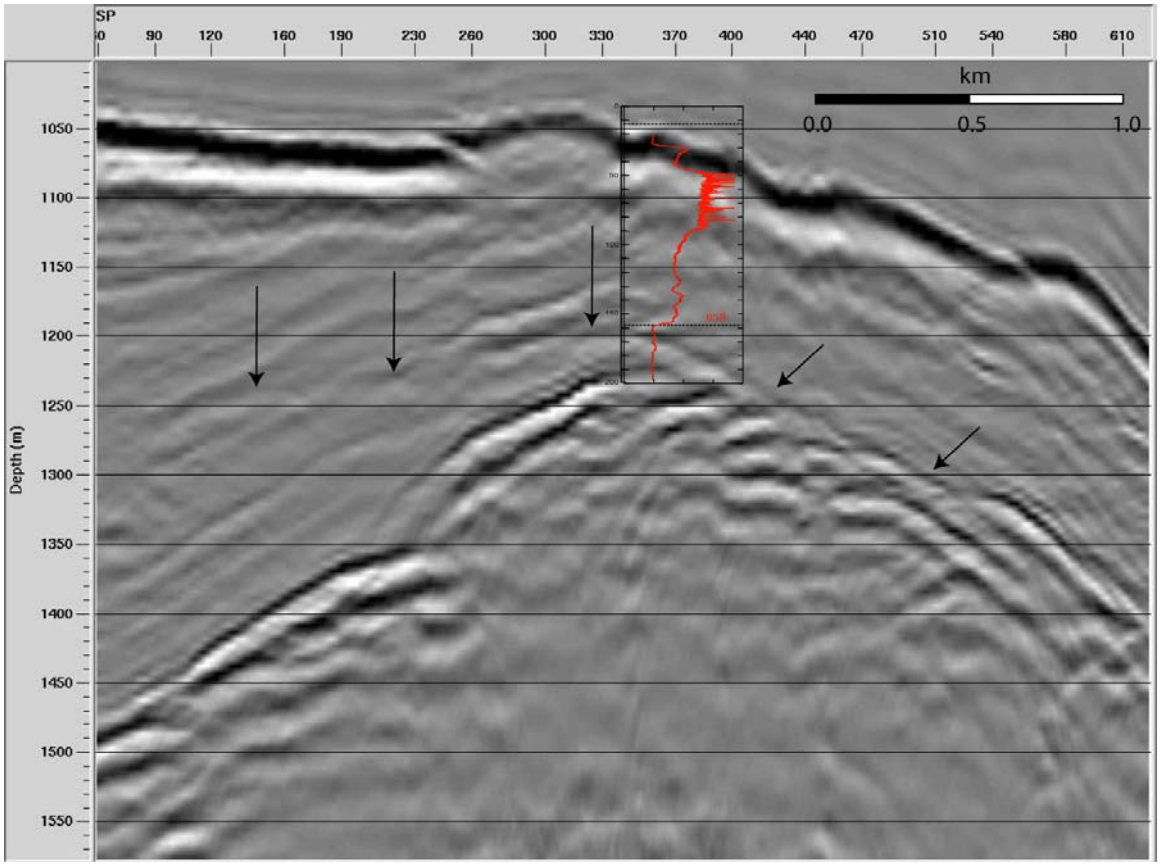

Figure 9.4 PSDM image with Well 10 resistivity log overlay. BSR is indicated with black arrows. Well 12 and 13 are currently being interpreted for BSR at NIO.

Future Work

The velocity model together with the PSDM image (Figure 9.5) suggest that an anomalous feature at the seafloor between CDP 230 and 340. This mound like feature shows chaotic seismic facies below the seafloor and lateral lowering in velocity. Low velocities, most likely free gas, are also closest to the seafloor below this mound like feature. It is possible that this is an active mound with gas seeps. Since Well 10, that has anomalously high hydrate content, is close to this mound like feature, further investigation of this feature can be important to the understanding of the hydrate distribution along the line.

The velocity model that has been determined though processing will be improved though joint inversion of reflection traveltimes (Jaiswal and Zelt 2008). The

resulting model will be used as a starting model for waveform inversion (Pratt 1999).

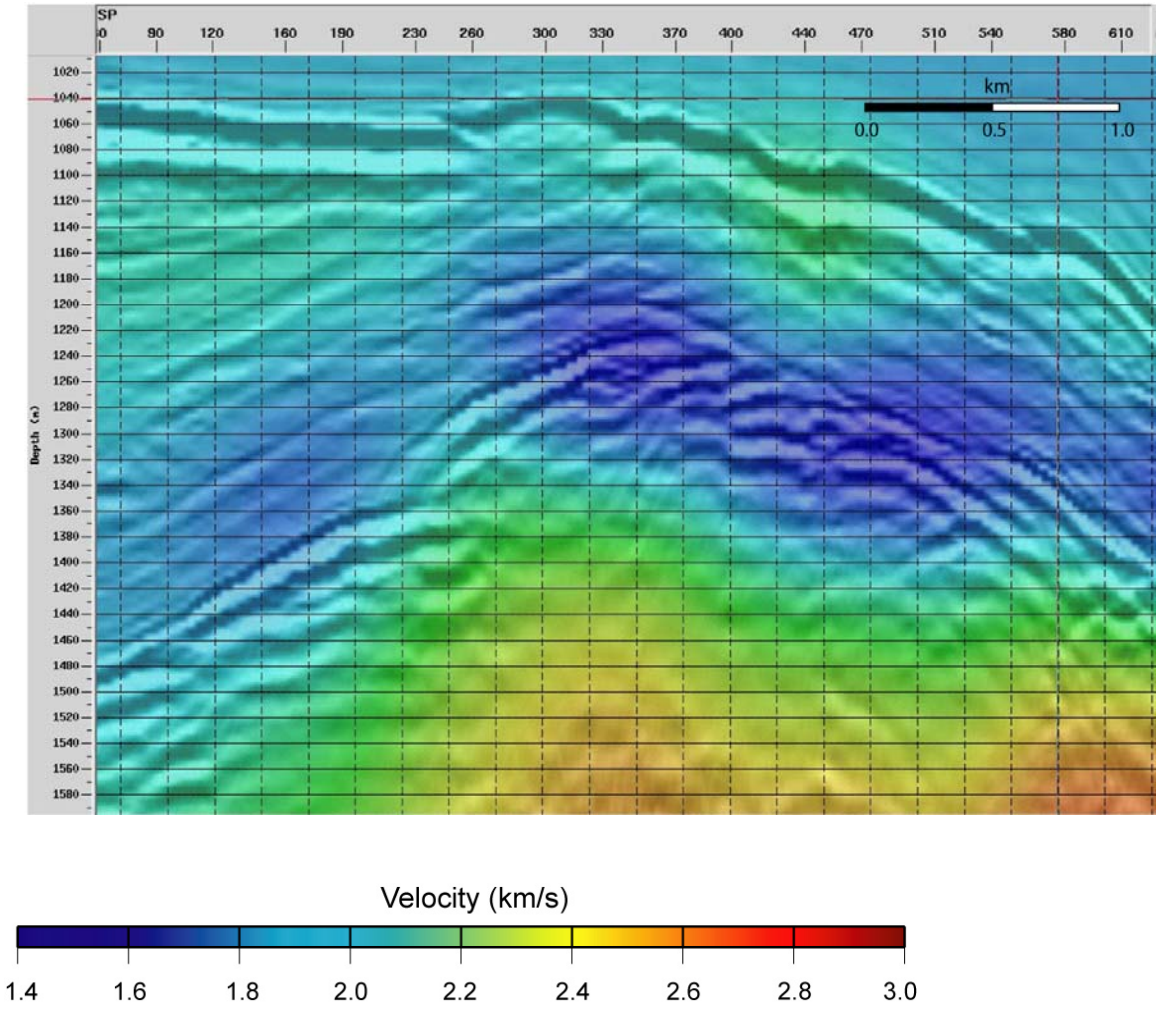

Figure 9.5 Overlay of PSDM image and velocity model. Low velocity zones, most likely representing free gas, are shallowest below the mound like feature (between CMPs 230 and 340).

References

Hale, D., 1984, Dip-moveout by Fourier-transform: Geophysics, 49, 741-757.

Jaiswal, P., and Zelt, C.A., Unified Imaging of Multichannel Seismic Data: Combining Traveltime Inversion and Pre-Stack Depth Migration, Geophysics, In Press.

Schneider, W. A., 1978, Integral formulation for migration in 2 and 3 dimensions: Geophysics, 43, 49-76.

Yilmaz, Ö., 2001, Seismic data processing (Investigations in Geophysics), 2 volumes: SEG.

Pratt, R. G., 1999, Seismic waveform inversion in the frequency domain, Part 1: Theory and verification in a physical scale model: Geophysics, 64, 888-901.

Task 10 Technology Transfer

ICGH 2008

Oral presentation, “Relating Gas Hydrate Saturations to Depth of Sulfate-Methane Transition,” G. Bhatnagar, W. Chapman, G. Dickens, B. Dugan, G. Hirasaki.

Poster, “Effect of Overpressure on Gas Hydrate Distribution,” G. Bhatnagar, W. Chapman, G. Dickens, B. Dugan, G. Hirasaki.

Abstracts submitted to the AGU meeting in San Francisco, December, 2008

Gas Production from Unconfined Hydrate reservoirs

J. Phirani, G. J. Hirasaki, K. K. Mohanty

Description of material: Large quantities of natural gas hydrates are present in marine sediments along the coastlines of many countries as well as in the arctic region. The production of gas from these naturally occurring gas hydrates is difficult due to complexity of thermodynamics and fluid flow involved in the process. This research is aimed at assessing production of natural gas from unconfined marine deposits of methane gas hydrates. An implicit, multiphase, multi-component, thermal, 3D simulator is used which can simulate formation and dissociation of hydrates in porous media in both equilibrium and kinetic modes. Three components (hydrate, methane and water) and four phases (hydrate, gas, aqueous-phase and ice) are considered. In this work we simulate depressurization and warm water flooding for gas production from hydrates in reservoirs underlain by an unconfined aquifer layer. Water flooding has been studied as a function of injection temperature, injection pressure, production pressure and degree of unconfinement.

Application: In order to produce gas from hydrates economically, efficient production techniques must be developed. Experiments on hydrates are difficult to perform; feasibility of production can be found from simulations. Hydrate reservoirs associated with unconfined aquifer beneath are not uncommon. The determination of injection and production conditions for these reservoirs through simulation will help in designing the effective production techniques.

Results and discussion: For the unconfined reservoirs associated with large aquifers the production by depressurization is inefficient. Water from the aquifer maintains the pressure in the reservoir except in the near-well regions. Warm water flooding is very effective in hydrate dissociation. Sensitivity of gas production to injection and production well conditions and degree of un-confinement has been studied.

Significant new contribution: Production strategies for unconfined hydrate reservoirs.

Effect of Lithologic Heterogeneities on Gas Hydrate Distribution

Sayantan Chatterjee, Gaurav Bhatnagar, Walter G. Chapman, Gerald R. Dickens, Brandon Dugan, George J. Hirasaki

Accumulation of gas hydrate and free gas is modeled in heterogeneous marine sediments over geologic time scales. Our two-dimensional models incorporate deposition and compaction of heterogeneous sediment, methane generation, and migration of water with dissolved gas, so we can study how focused fluid flow through a vertical fracture network and/or high permeability sand layers affects regional and local hydrate accumulation and saturation. The focused fluid flow is visualized by vector field plots. Simulations with a vertical fracture network, 100 times more permeable than the surrounding formation that extends through the gas hydrate stability zone (GHSZ) up to the seafloor show focused fluid flow causing relatively higher hydrate and free gas saturation within the fracture network compared to the surrounding, lower permeability formation. Systems with dipping sand layers show similar localized, enhanced concentrations of hydrate and free gas within the high permeability conduits. Anisotropic cases with lower ratio of vertical to horizontal permeability, k_v/k_h (order of 10^{-2}), show relatively higher hydrate saturations within the high permeability conduits because anisotropy focuses more of the fluid into the high permeability conduit. Cases where vertical fracture networks cut through sand beds will also be discussed. In our previous **one-dimensional** work, we found that the accumulated hydrate saturation was dependent on Peclet number, Pe, which is the ratio of convective flux to the diffusive flux of methane. In our current two-dimensional work, it is the **local** convective flux relative to diffusion that determines the magnitude of hydrate and free gas saturation.

Extending Nuclear Magnetic Resonance Data for Permeability Estimation in Fine-Grained Sediments

Hugh Daigle and Brandon Dugan, Department of Earth Science, Rice University, Houston, Texas, USA

We developed a method for using nuclear magnetic resonance (NMR) T_2 data and gamma ray data to estimate lithology-dependent permeability in silt- and clay-rich sediments. This model, based on the Schlumberger-Doll Research (SDR) model, allows for high resolution (<1 m) permeability estimates throughout a logged interval. Our model was calibrated using direct measurements on core samples from Keathley Canyon Lease Block 151 in the northern Gulf of Mexico. From NMR and gamma ray data we are able to determine permeability from 10^{-18} to 10^{-14} m^2 (0.001 to 10 millidarcies). Thus from discrete core samples and log data we were able to develop a permeability model for the entire sedimentary column (425 m). Lithologic variation was incorporated into the model by varying the *A* coefficient based on the gamma ray response. This provides a more accurate permeability model than assigning a constant value to *A* as is typically done. The relationship between *A* and intrinsic lithologic properties is unclear; simple pore system models suggest that *A* may be related to specific surface,

tortuosity, and pore structure; we investigate simple models to quantify how these properties vary with sediment consolidation and what their relationship is to *A*. A comprehensive understanding that links NMR data and *A* to pore-scale properties will provide new constraints on deformation and flow in porous systems, and will contribute to our understanding of sediment properties for fluid flow modeling at local and regional scales.

Compositional Effect on Hydrate/Free Gas Transition and BSR

Guangsheng Gu, Priyank Jaiswal, Walter Chapman, Colin Zelt, and George J Hirasaki

Abstract

Gas hydrate is often characterized in remote detection by seismic profiles and Bottom-Simulating Reflector (BSR), which is due to an abrupt acoustic impedance contrast between the base of gas hydrate stability zone (GHSZ) and free gas layer below. However, in some cases, hydrate is present but BSR is not observed. We hypothesize that multi-hydrocarbon components in a hydrate system can induce gradual transition of hydrate/free gas saturations, and result in a weak seismic reflection.

In this work, we demonstrate that a small fraction of heavier hydrocarbon component can induce a gradual transition of hydrate/free gas saturations in sediment over a significant distance (relative to acoustic wavelength). If the thermogenic gas source from deeper sediment contains 5% (mol/mol) propane, a transition zone as thick as ~50 m can be formed, in which hydrate, gas, and aqueous phases can co-exist. The saturations of each phase change gradually, causing a gradual transition of acoustic impedance. Seismic waves with different characteristic wavelengths are tested to generate synthetic seismic responses. Results show that, if the ratio of characteristic wavelength to thickness of transition zone (λ/L_{trans}) is less than 1, then the reflection is very weak; if the ratio is much higher than 1, the reflection is very strong. This indicates that in the case of a multi-hydrocarbon hydrate system, the reflection response is dependent on the thickness of transition zone and seismic wavelength. This provides a possible mechanism why in some places hydrate is present but BSR is not observed.

Phase 3

COST PLAN / STATUS								
	Phase 1	Phase 2	Phase 3 7/01/08-6/30/09				Phase 3	
Baseline Quarter Reporting			7/1/08 - 9/30/08	10/1/08 - 12/31/08	1/1/09 - 3/31/09	4/1/09 - 6/30/09	Totals	Cumulative Totals
Baseline Cost Plan Allocation (SF- 424A)								
Federal Share	$ 3,624	$320,010	$ 82,784	$ 82,784	$ 82,784	$ 82,784	$ 331,135	$ 654,769
Non-Federal Share	$ 1,004	$114,612	$ 26,908	$ 26,908	$ 26,908	$ 26,908	$ 107,630	$ 223,246
Total Planned	$ 4,628	$434,623	$ 109,691	$ 109,691	$ 109,691	$ 109,691	$ 438,765	$ 878,016
Cumulative Baseline Cost	$ 4,628	$439,251	$ 548,942	$ 658,634	$ 768,325	$ 878,016	$1,316,781	$ 1,760,660
Actual Incurred Cost								
Federal Share	$ 3,082	$298,506	$ 71,995					$ 316,637
Non-Federal Share	$ 1,091	$118,145	$ 15,049					$ 134,285
Total Incurred	$ 4,173	$416,651	$ 87,044					$ 507,868
Cumulative Costs	$ 4,173	$420,824	$ 507,868					$ 932,865
Variance (plan-actual)								
Federal Share	$ 542	$ 21,504	$ 10,789					$ 32,835
Non-Federal Share	$ (87)	$ (3,533)	$ 11,859					$ 8,238
Total Variance	$ 455	$ 17,971	$ 22,647					$ 41,073
Cumulative Variance	$ 455	$ 18,426	$ 41,073					$ 59,954

Milestone Plan/Status

Task	Milestone: Status and Results	Date	Status
5. Carbon inputs and outputs to gas hydrate systems	5.1a Measure iodine in sediments We have measured iodine concentrations in pore waters from several gas hydrate systems. The analyses are completed and we are writing the results over the summer.	12/07	1/08
	5.1b Constrain C_{org} inputs from iodine We will measure the content and isotopic composition of organic carbon and carbonate in sediment from cores of several gas hydrate systems. We have collected most of the samples, although plan to visit the ODP repository (College Station) in late spring or early summer to collect additional samples. Some analyses have been completed; additional ones will be done over the summer.	10/08	
	5.2a Construct metal profiles in sediments We will measure metal contents in sediment from cores of several gas hydrate systems to constrain past hydrocarbon outputs via anaerobic oxidation of methane (AOM). Some work was published in the fall (Snyder et al., 2007). We plan on submitting a manuscript regarding profiles on the Peru Margin by the end of summer.	12/09	
	5.2b Modeling/integrating profiles We will use the metal and iodine profiles to constrain models for gas hydrate formation. We have discussed data and models but have not begun this work so far.	12/10	
6. Numerical models for quantification of hydrate and free gas accumulations	6.1 Model development. The recipient shall develop finite difference models for the accumulation of gas hydrate and free gas in natural sediment sequences on geologically relevant time scales.	9/07	1/08
	6.2: Conditions for existence of gas hydrate	3/07	done

	The recipient shall summarize, quantitatively, the conditions for the absence, presence, and distribution of gas hydrates and free gas in 1-D systems by expressing the conditions in terms of dimensionless groups that combine thermodynamic, biological and lithologic transformation, and transport parameters.		
	6.3 Compositional effect on BSR The recipient shall add to the numerical model, developed under this task, a chloride balance and multi-hydrocarbon capability specifically to investigate how hydrocarbon fractionation might affect Bottom Simulating Reflectors (BSRs).	7/07	6/09
	6.4: Amplitude Attenuation and chaotic zones due to hydrate distribution The recipient shall simulate preferential formation of gas hydrate in coarse-grained, porous sediment in 2-D by linking fluid flux to the permeability distribution.	3/09	started
	6.5: Processes leading to overpressure The recipient shall quantify, by simulation and summarize by combination of responsible dimensionless groups, the conditions leading to overpressure to the point of sediment failure.	3/08	done
	6.6 Concentrated hydrate and free gas The recipient shall, using 2-D and 3-D models, simulate lateral migration and concentration of gas hydrate and free gas in structural and stratigraphic traps.	3/08	started
	6.7 Focused free gas, heat and salinity The recipient shall quantify, using 2-D and 3-D model simulations and comparisons to available observations, the factors controlling the process of localized upward migration of free gas along faults and lateral transfer to dipping strata that can lead to chaotic zones and possible accumulations of concentrated hydrate.	9/09	
	6.8 Sulfate profile as indicator of methane flux	7/07	done

	The recipient shall compute, for systems where data on the sulfate profile is available, the oxidation of methane by sulfate and shall indicate the perceived level of effect on gas hydrate accumulation and the data's value as an indicator of methane flux.		
	6.9 Application of models to interpretation of case studies. The models developed in Task 6 will be applied to case studies in the interpretation of each of the other tasks.	6/10	6/10
7. Analysis of production strategy	7.1a Pore scale model development and Hydrate code comparison For this milestone, we will develop pore-scale models of hydrate accumulation by simulation. Our hydrate code will be used to solve a set of problems formulated by the Code Comparison Study group. Our results will be compared with those of other hydrate codes. Should be changed to: 6/08 Reason: The starting date was moved to 6/07 Status: Code comparison study is 80% complete.	1/08	6/08 Code comparison is done.
	7.1b Petrophysical and thermophysical properties of hydrate sediments from pore-scale model For this milestone, we will assume the pore-scale models of hydrate accumulation developed in the last milestone and estimate transport properties as a function of hydrate and gas saturations. Should be changed to: 6/09 Reason: The starting date was moved to 6/07 Status: Have not started	1/09	6/09
	7.2a Modeling of several production strategies to recover gas from marine hydrates Several production strategies would be modelled using the transport property correlations developed in the previous milestone. Optimal strategies will be identified. Should be changed to: 6/10	1/10	6/10

	Reason: The starting date was moved to 6/07 Status: Have not started		
	7.2b Effect of marine reservoir heterogeneities on production of methane Reservoir heterogeneity anticipated in marine environments (known or determined through other tasks) would be incorporated. Appropriate hydrate distributions, either constrained from experimental data or mechanistic simulations (Task 5) would be used. Sensitivity of gas production to the heterogeneities would be calculated. Should be changed to: 6/11 Reason: The starting date was moved to 6/07 Status: Have not started	12/10	6/10
8. Seafloor and borehole stability	8.1a Collection of data We have collected the published data and are working it into a data base. We are also working on a review paper summarizing the state of the art settings. This will include laboratory experiments, field data, published results, and unpublished data.	05/08	Completed
	8.1c Complete database We are organizing the data from task 8.1a into a format that can be searched and used by researchers trying to understand mechanical behavior of hydrate-bearing sediment. We will also identify key gaps in the database for focusing future hydrate research endeavors. We have started exchanging these data with the modeling components of this project.	10/09	On target
	8.2a Link database with models We have started passing data along to the modeling groups so they can use sediment properties from hydrate provinces as they simulate hydrate accumulation and production.	08/08	On target
	8.2b Add sediment stability to models Standard stability calculations have been implemented in a standard basin model. Now that it is functional we will work with the hydrate accumulation model to add a stability calculation to the 2-D models.	10/08	On target

	8.2c Conditions for (in)stability After implementing the stability model in the hydrate accumulation code, we can explore the conditions (e.g., hydrate dissociation, sea-level fall) that could drive slope failure and hydrate/methane release or lead to borehole failures during production.	9/09	On target
9 Geophysical imaging of hydrate and free gas	9.1 Preliminary processing and inversion of seismic data. Perform conventional seismic reflection processing, velocity analysis, travel time tomography, and other analyses as deemed appropriate and necessary.	8/08	
	9.2: Final 1-D elastic and 2-D acoustic waveform inversion. Apply 1-D elastic and 2D acoustic inversions on data obtained from subtask 9.1 to derive determine high-resolution elastic and acoustic properties.	8/09	
	9.3: Rock physics modeling. Apply rock physics models to the developed seismic models to estimate hydrate saturation and lithology through application of well log data in conjunction with data from subtask 9.2. For this subtask we shall seek to collaborate with research being conducted under separately funded DOE-NETL projects (DE-FC26-05NT42663 with Stanford University, "Seismic-Scale Rock Physics of Methane Hydrate" and others as applicable).	8/10	

National Energy Technology Laboratory

626 Cochrans Mill Road
P.O. Box 10940
Pittsburgh, PA 15236-0940

3610 Collins Ferry Road
P.O. Box 880
Morgantown, WV 26507-0880

One West Third Street, Suite 1400
Tulsa, OK 74103-3519

1450 Queen Avenue SW
Albany, OR 97321-2198

539 Duckering Bldg./UAF Campus
P.O. Box 750172
Fairbanks, AK 99775-0172

Visit the NETL website at:
www.netl.doe.gov

Customer Service:
1-800-553-7681